Gondwana Research 33 (2016) 4–23

Contents lists available at ScienceDirect

Gondwana Research

journal homepage: www.elsevier.com/locate/gr

GR Focus Review

Geophysical constraints on geodynamic processes at convergent margins: A global perspective

I.M. Artemieva [a,*], H. Thybo [a], A. Shulgin [b]

[a] Geology Section, IGN, University of Copenhagen, Øster Voldgade 10, Copenhagen 1350, Denmark
[b] Centre for Earth Evolution and Dynamics (CEED), University of Oslo, P.O. Box 1028 Blindern, NO-0315 Oslo, Norway

ARTICLE INFO

Article history:
Received 7 April 2015
Received in revised form 22 June 2015
Accepted 23 June 2015
Available online 6 August 2015

Handling Editor: M. Santosh

Keywords:
Plate boundaries
Subduction zone
Dip angle
Seismicity
Heat flow
Gravity

ABSTRACT

Convergent margins, being the boundaries between colliding lithospheric plates, form the most disastrous areas in the world due to intensive, strong seismicity and volcanism. We review global geophysical data in order to illustrate the effects of the plate tectonic processes at convergent margins on the crustal and upper mantle structure, seismicity, and geometry of subducting slab. We present global maps of free-air and Bouguer gravity anomalies, heat flow, seismicity, seismic Vs anomalies in the upper mantle, and plate convergence rate, as well as 20 profiles across different convergent margins. A global analysis of these data for three types of convergent margins, formed by ocean–ocean, ocean–continent, and continent–continent collisions, allows us to recognize the following patterns. (1) Plate convergence rate depends on the type of convergent margins and it is significantly larger when, at least, one of the plates is oceanic. However, the oldest oceanic plate in the Pacific ocean has the smallest convergence rate. (2) The presence of an oceanic plate is, in general, required for generation of high-magnitude ($M > 8.0$) earthquakes and for generating intermediate and deep seismicity along the convergent margins. When oceanic slabs subduct beneath a continent, a gap in the seismogenic zone exists at depths between ca. 250 km and 500 km. Given that the seismogenic zone terminates at ca. 200 km depth in case of continent–continent collision, we propose oceanic origin of subducting slabs beneath the Zagros, the Pamir, and the Vrancea zone. (3) Dip angle of the subducting slab in continent–ocean collision does not correlate neither with the age of subducting oceanic slab, nor with the convergence rate. For ocean–ocean subduction, clear trends are recognized: steeply dipping slabs are characteristic of young subducting plates and of oceanic plates with high convergence rate, with slab rotation towards a near-vertical dip angle at depths below ca. 500 km at very high convergence rate. (4) Local isostasy is not satisfied at the convergent margins as evidenced by strong free air gravity anomalies of positive and negative signs. However, near-isostatic equilibrium may exist in broad zones of distributed deformation such as Tibet. (5) No systematic patterns are recognized in heat flow data due to strong heterogeneity of measured values which are strongly affected by hydrothermal circulation, magmatic activity, crustal faulting, horizontal heat transfer, and also due to low number of heat flow measurements across many margins. (6) Low upper mantle Vs seismic velocities beneath the convergent margins are restricted to the upper 150 km and may be related to mantle wedge melting which is confined to shallow mantle levels.

Contents

* Corresponding author.
E-mail addresses: irina@ign.ku.dk (I.M. Artemieva), thybo@ign.ku.dk (H. Thybo), alexey.shulgin@geo.uio.no (A. Shulgin).

http://dx.doi.org/10.1016/j.gr.2015.06.010
1342-937X/

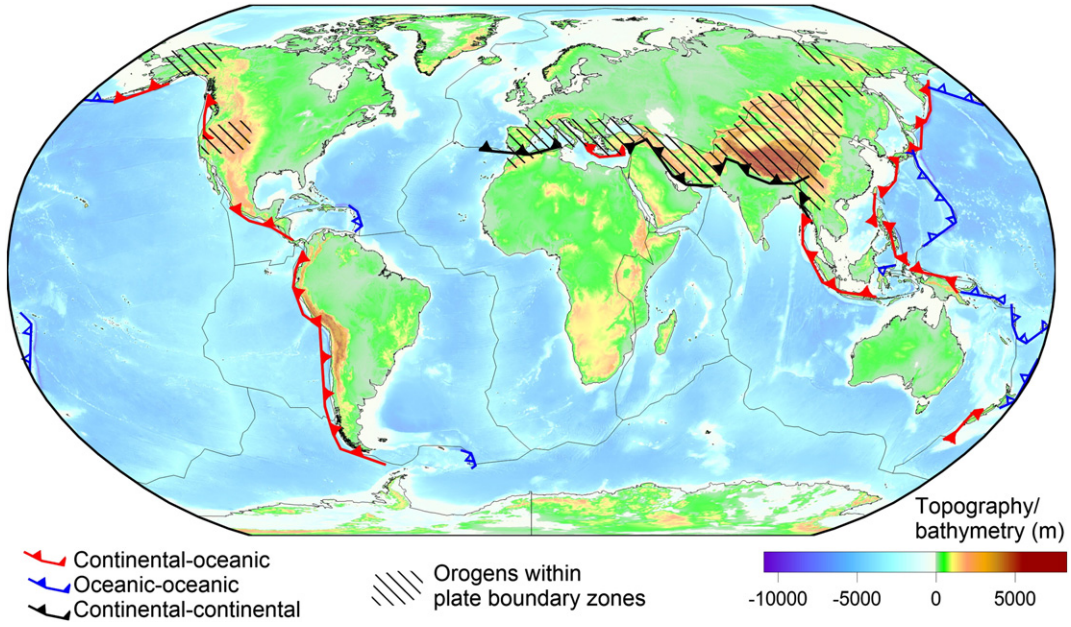

Fig. 1. Global distribution of convergent margins of different types. Topography and bathymetry based on ETOPO1 (Amante and Eakins, 2009).

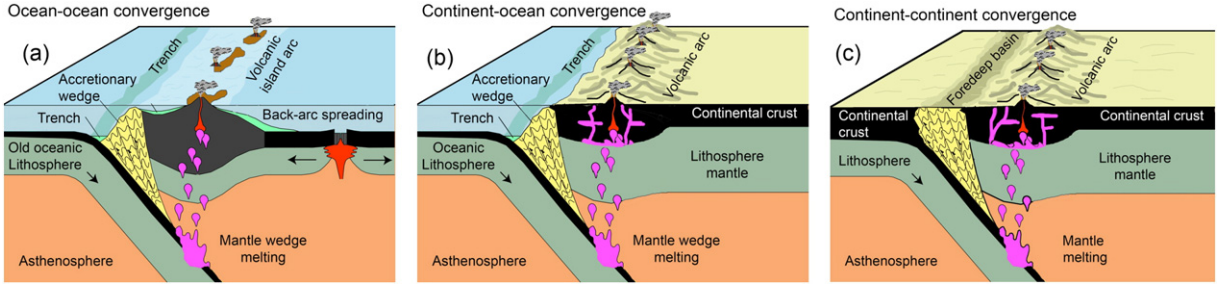

Fig. 2. Sketches of three major types of convergent margins.

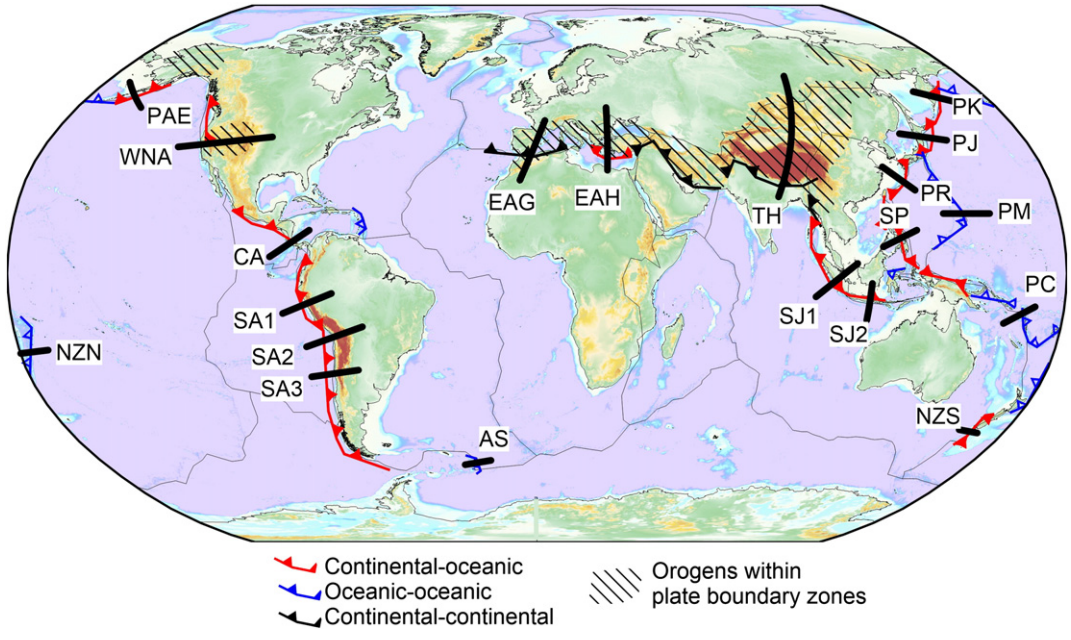

Fig. 3. Profiles across the convergent margins (illustrated in Fig. 4). See Table 1 for details.

Table 1
Major characteristics of convergent margins discussed in text.

Profile in Fig. 3	Location	Tectonic setting	Type of conv. margin	Convergence rate (cm/y)[a]	Subduction angle, sub-Moho (deg)[b]	Subduction angle, deep (deg)[b]	Age of subducting oceanic plate (Ma)	Seismicity range (km)
WNA	Western North America	The Cascadia subduction zone: the oceanic Juan de Fuca and Gorda Plates subduct beneath the continental North American plate; further south it forms the zone of orogeny within the Western USA	OC, PBZ	2.3	–	–	10	Crustal
SA1	South America-Andes	The oceanic Nazca Plate subducts beneath the continental South American Plate along the Peru–Chile Trench	OC	6.8	13	70	25	<200, 515–650
SA2				7.2	30	?	40	<290, 580–610
SA3				7.4	13	?	35	<200, 575–620
AS	South Atlantics-Sandwich	The oceanic South American Plate subducts beneath the South Sandwich Plate (composed of oceanic lithosphere with continental fragments), forming the South Sandwich Trench	OO or OC	5.7	40	?	70	<170, 270–310
CA	Pacific Central America	The oceanic Cocos Plate subducts under the Caribbean Plate and forms the Middle America Trench	CO	7.8	?	?	15	<95, 205
PAE,	North Pacific, the Aleutians	The oceanic Pacific Plate subducts under the continental segment of the North American Plate along the Aleutian Trench (PAE); further west, the Pacific Plate subducts under the oceanic segment of the North American Plate (PAW)	OC	6.6	11	90	55	<230
PJ	West Pacific (PJ = Japan,	The oceanic Pacific plate subducts beneath the continental Amurian and	OC	9.4	23	32	130	<230, 310–410
PK	PK = Kamchatka)	Okhotsk Plates (parts of the Eurasian Plate) at the Japan and Kuril Trenches	OC	8.1	40	65	100	<190, 310, 490, 610–660
PR	West Pacific, Ryukyu	The oceanic Philippine Sea Plate subducts beneath the continental Eurasian Plate at the Ryukyu Trench	OC	7.9	53	–	50	<250
PM	West Pacific, Mariana	The oceanic Pacific Plate subducts under the oceanic Philippine Sea Plate at the Mariana Trench	OO	2.7	27	70	160	<260, 310, 410–610
SP	West Pacific, Philippines	The continental Sunda Plate subducts under the Philippine Mobile Belt at the Negros and the Cotabato Trenches, while the continental Eurasian Plate subducts under the Philippine Mobile Belt at the Manila Trench. On the eastern side of the Philippines, the direction of subduction reverses: the oceanic Philippine Sea Plate subducts under the Philippine Mobile Belt at the Philippine and East Luzon Trenches	CC or OC	10.0	36	75	50	<160, 220–240, 525–615
SJ1	Indian ocean, Sunda-Java	The oceanic Indo-Australian Plate subducts beneath the continental Sunda	OC	4.8	25	?	50	<235, 585
SJ2		Plate along the Sunda Trench		4.9	25	90	130	<185, 520–640
NZS	New Zealand (NZS	South-west of New Zealand: the Indo-Australian Plate subducts	OC?	3.4	?	?	65	<50, 100
NZN	= South Island; NZN = North Island)	under the oceanic Pacific Plate (NZS). North-east of New Zealand the direction of subduction reverses: the oceanic Pacific Plate subducts under the Indo-Australian Plate (note that E–W are flipped on profile NSN in Fig. 10).	OO	7.2	43	74	95	0–650
PC	Pacific, New Caledonia	The oceanic Indo-Australian Plate subducts beneath the oceanic Pacific Plate	OO	9.2	50	85	20	<340
EAG	Mediterranean Europe	Broad band of diffuse deformation caused by the collision of the	PBZ	0.5	–	–	–	Crustal, 600
EAH	(EAG = Gibraltar arc–Pyrenees; EAH = Hellenic arc–Carpathians)	continental African and Eurasian Plates, with numerous subduction zones and the orogenic belt that extends from the Atlantic coast through the Mediterranean region (Alps, Carpathians, Pyrenees, Apennines, Dinarides, Atlas, Balkans, Caucasus) to Zagros and Anatolia. Profile EAG crosses the Gibraltar arc and the Pyrenees. In some parts of the Mediterranean Sea, oceanic lithosphere subducts under the continental Eurasian Plate (the Hellenic arc, profile EAH, which further crosses the Vrancea zone in the Carpathians).	CC	1.0	13	51	200?	<180
TH	Tibet-Himalayas-Central Asia	Broad band of diffuse deformation caused by the collision of the continental Indian and Eurasian Plates, which includes the Himalayas, Tibet (under which the Indian Plate subducts under the Eurasian Plate), the orogenic belts of the Central Asia and the Indonesian Archipelago	PBZ, CC	4.6	–	–	–	Crustal

[a] Convergence rate is based on MORVEL plate velocity model (DeMets et al., 2010).
[b] Subduction dip is calculated from the geometry of the seismogenic zone (Fig. 4).

1. Introduction

Convergent boundaries, together with divergent and transform boundaries, form three major types of boundaries between the lithospheric plates (Figs. 1, 2). Given that most disastrous tectonic activity, expressed in seismicity and volcanism, is associated with the convergent boundaries along oceanic margins, they are also termed active margins; however active margins do not include all of the convergent boundaries. Due to strong tectonic activity and associated geohazards, active margins have been a focus of numerous studies and dedicated research programs. Collisional orogens associated with convergent boundaries further host numerous mineral resources and, being important from economic perspective, are a focus of academic and industry studies (e.g. UNESCO Project 600).

Convergent margins are defined as boundaries between the colliding lithospheric plates. Depending on the nature of the plates, three types of convergent margins are commonly recognized (Figs. 1–2): ocean–ocean, continent–ocean, and continent–continent. The two latter

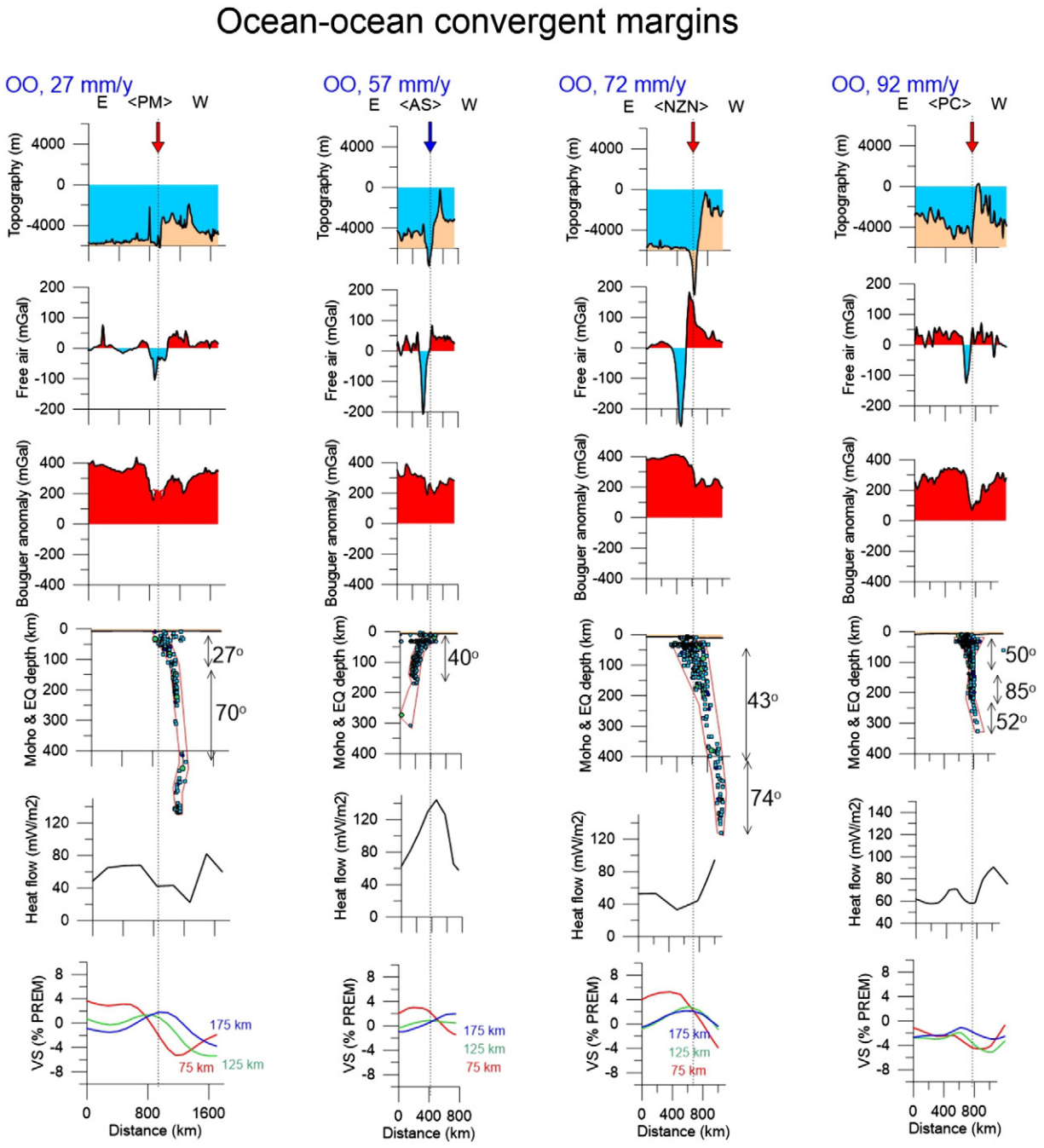

Fig. 4. Twenty profiles across different types of convergent margins (see Fig. 3 for locations), which show from top to bottom: (i) variations in topography (based on ETOPO1, Amante and Eakins, 2009), (ii) free air (based on EGM2008, Pavlis et al., 2012) and (iii) Bouguer gravity anomalies, (iv) depth to Moho and seismicity (Mw > 4.0, within a 400 km-wide corridor along the profiles, based on ISC-GEM catalogue, Storchak et al., 2013), (v) heat flow (based on compilation of IHFC, 2011), and (vi) upper mantle Vs velocity at depths of 75 km, 125 km, and 175 km (based on tomography model of Schaeffer and Lebedev, 2013). To simplify comparisons, all profiles are presented with the subduction direction from left to right. Red arrows on the top and vertical lines mark the position of the convergent boundaries (trenches) (in few cases of several subductions along a profile, blue arrows mark the subduction directed from right to left). Slabs are outlined based on seismicity, dip angle is indicated at seismicity plots as calculated for the depth range marked by black arrows. All profiles have the same vertical and horizontal scales. Index on the top marks the type of convergent margin (OO = ocean–ocean, CO = continent–ocean, CC = continent–continent, the number–convergence rate, <code> refers to profile label in Fig. 3 and Table 1).

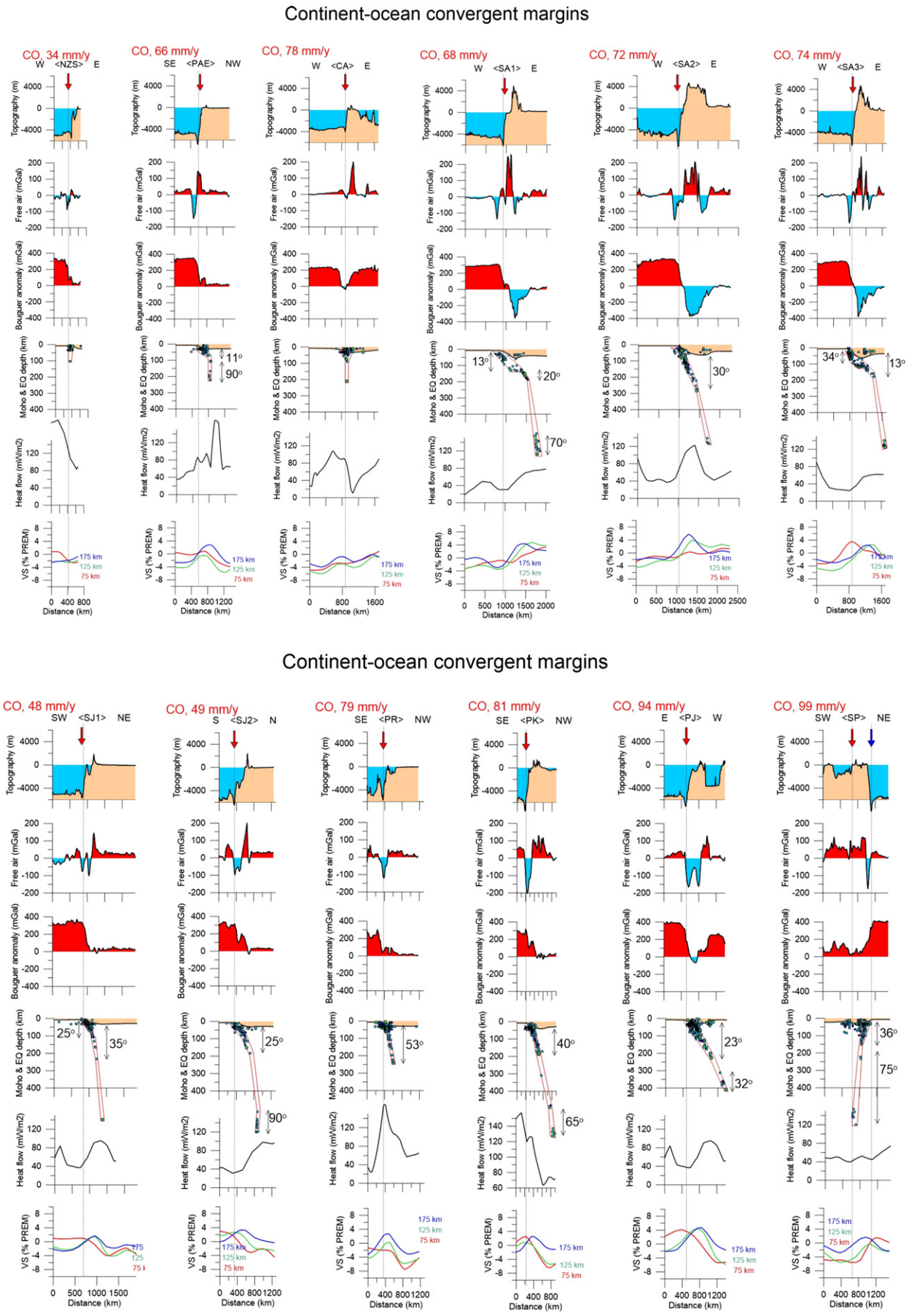

Fig. 4 (*continued*).

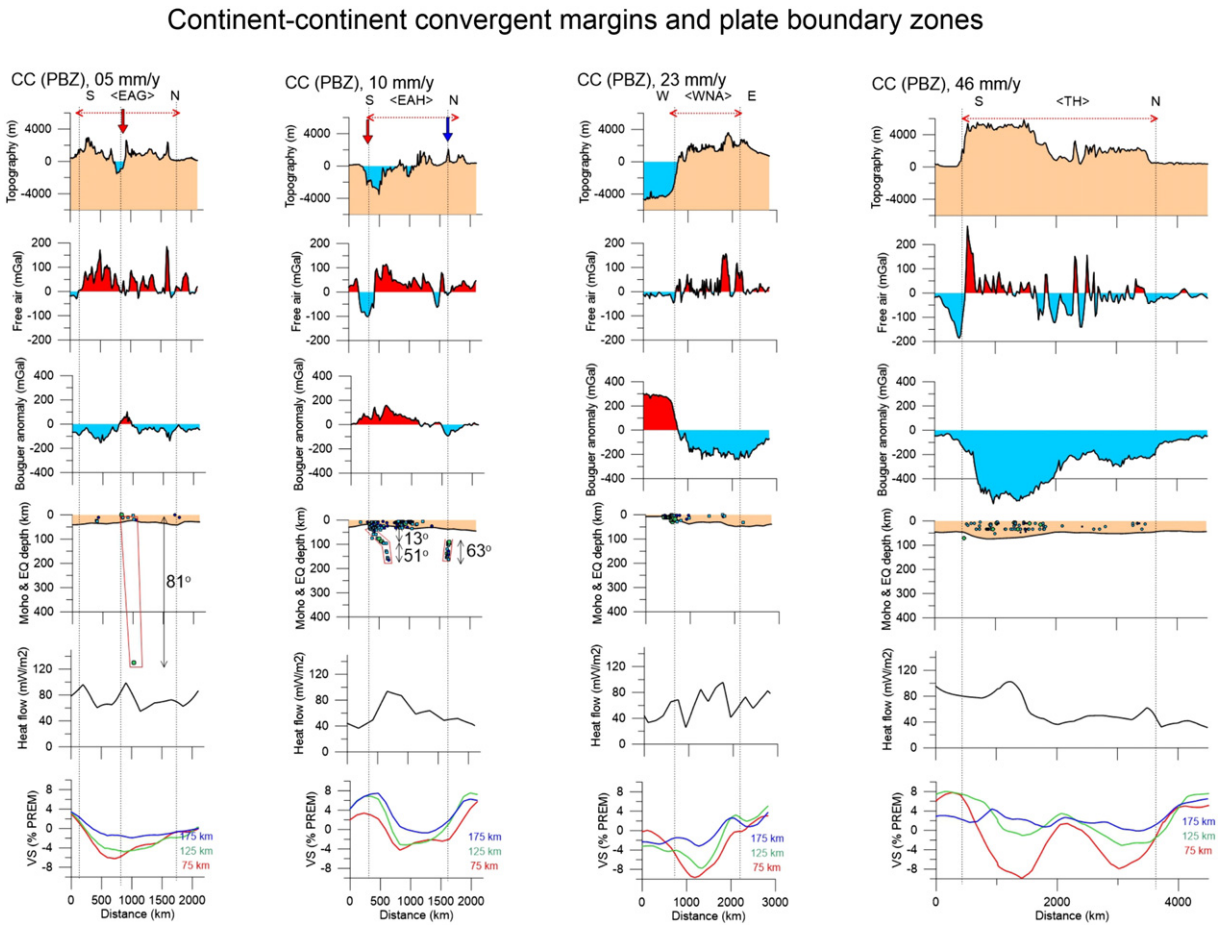

Fig. 4 (*continued*).

types, in particular continent–continent collision, often form a zone of distributed deformation within the continental interior (plate boundary zone, PBZ). In some cases, convergent boundaries may form a zone of diffuse deformation where the plate boundary is not clearly expressed (Zatman et al., 2004). Some convergent margins may be dormant, such as the speculative plate boundary across Siberia, which starts at

Table 2
Key references to convergent margins discussed in text.

Location	Selected key references
Western North America	Green et al. (1986), Hyndman et al. (1990), Trehu et al. (1994), Calvert (1996), Brocher et al. (2003), Nicholson et al. (2005), Madsen et al. (2006), Bostock (2013)
South America (the Andes)	ANCORP Working Group (1999), Yuan et al. (2000), Schurr et al. (2006), Gilbert et al. (2006), Contreras-Reyes et al. (2008), Audet et al. (2009)
South Atlantics (the Sandwich arc)	Larter et al. (2003), Li et al. (2008), Dalziel et al. (2013)
Pacific Central America	Johnston and Thorkelson (1997), Zelt et al. (1999), Götze and Krause (2002), Rogers et al. (2002), Trenkamp et al. (2002), Grevemeyer et al. (2007), Kim et al. (2010)
North Pacific (the Aleutians)	Holbrook et al. (1999), Gorbatov et al. (2000), Lizarralde et al. (2002), Eberhart-Philips et al. (2006), Jicha et al. (2006), Rondenay et al. (2008)
West Pacific (Japan, Kamchatka)	Suyehiro et al. (1996), Taira et al. (1998), Levin et al. (2002), Jiang et al. (2009), Nakanishi et al. (2009), Nakamura et al. (2014)
West Pacific (the Ryukyu arc)	Park et al. (1998), Font et al. (2001), Lallemand et al. (2001), McIntosh et al. (2005), Chou et al. (2009), Wu et al. (2009)
West Pacific (the Mariana arc)	Nagumo et al. (1981), Widiyantoro et al. (1999), Kárason and Van Der Hilst (2000), Calvert et al. (2008), Takahashi et al. (2008), Contreras-Reyes et al. (2011), Stratford et al. (2015)
West Pacific (the Philippines)	Kodaira et al. (2000), McIntosh et al. (2005), Nishizawa et al. (2007), Hirose et al. (2008), Matsubara et al. (2008), Eakin et al. (2014)
Indian ocean (Sunda-Java)	Kopp et al. (2011), Hall and Spakman (2002), Replumaz et al. (2004), Wagner et al. (2007), Spakman and Hall (2010), Lüschen et al. (2011), Shulgin et al. (2009, 2011, 2013)
New Zealand (NZS = South Island; NZN = North Island)	NZS: Eberhart-Phillips and Bannister, 2002; Okaya et al., 2002; Van Avendonk et al., 2004; Fry et al., 2014 NZN: Stern et al., 1987; Eberhart-Phillips and Reyners, 1999; Reyners et al., 2006; Stern et al., 2015
South-west Pacific (New Caledonia)	Pascal et al. (1973), Aitchison et al. (1995), Lagabrielle et al. (2005), Fichtner et al. (2010)
Mediterranean Europe (the Gibraltar arc–Pyrenees; the Hellenic arc–Carpathians–Alps)	Spakman et al. (1988), Platt and Vissers (1989), Spakman et al. (1993), Houseman and Molnar (1997), Mezcua and Rueda (1997), Wortel and Spakman (2000), Vacher and Souriau (2001), Lippitsch et al. (2003), Brückl et al. (2007), Souriau et al. (2008), Starostenko et al. (2013), Bokelmann and Rodler (2014), Levander et al. (2014), Morais et al. (2015), Qorbani et al. (2015)
Tibet, Himalayas, the Central Asia	Stauffer (1993), Kosarev et al. (1999), Zhao et al. (2001), Kind et al. (2002), Tilmann et al. (2003), Wittlinger et al. (2004), Yao et al. (2006), Zhang et al. (2012)

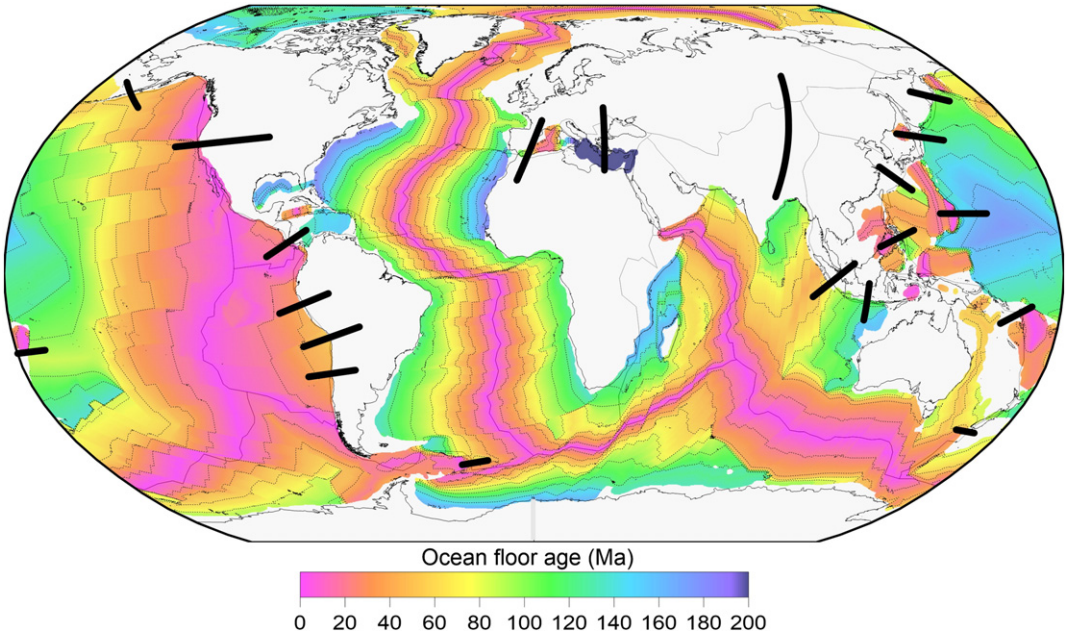

Fig. 5. Age of the ocean floor (based on Mueller et al., 2008). Black lines — profiles across the convergent margins discussed in the text (Table 1).

the Laptev sea of the Arctic shelf in the north and terminates at the Okhotsk sea in the south and separates the Siberian craton from the Verkhoyansk Fold Belt.

The present study provides a global comparative overview of convergent margins of the three types, without discussing specific details for any of the margins. Our motivation is to recognize major characteristics for each of the convergent margin types, based on the analysis of topography/bathymetry, gravity, heat flow, crustal structure, seismic structure of the mantle, seismicity patterns, slab dip angle, and plate convergence rate. We discuss global patterns and illustrate our analysis by a set of global maps for these parameters. We also present 20 geophysical cross-sections across different types of convergent margins world-wide (see Fig. 3 for locations); their major characteristics are presented in Table 1 and are illustrated in Fig. 4. For details on particular convergent boundaries readers are referred to regional studies with key references listed in Table 2; their overview is outside the scope of this paper (with the vast literature on the topic (e.g. Schellart and Rawlinson, 2010), such an overview cannot fit journal page limits).

2. Tectonic and topographic expression of convergent boundaries

All three types of convergent margins are associated with subduction zones. In case of ocean–ocean subduction, it is the older oceanic plate with colder and thicker lithosphere that subducts beneath younger and lighter oceanic plate (Fig. 5). An illustration of this pattern is the subduction of the old oceanic Pacific Plate under the young oceanic Philippine Sea Plate at the Mariana Trench (PM in Fig. 5). In case of continent–ocean collision, the oceanic plate subducts beneath the

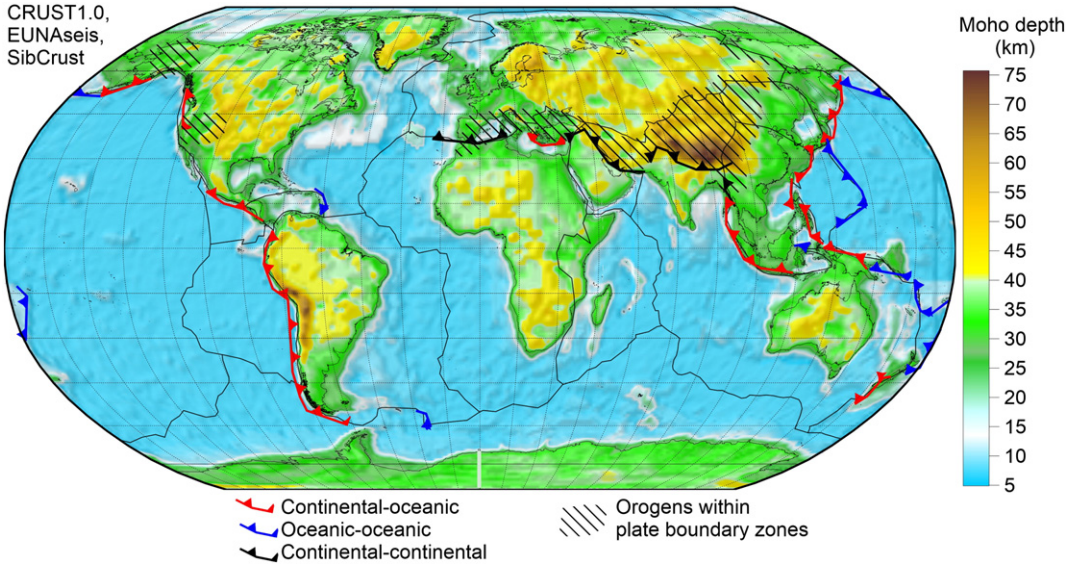

Fig. 6. Depth to Moho (based on EUNAseis (Artemieva and Thybo, 2013) and SibCrust (Cherepanova et al., 2013) regional crustal models for Eurasia and on CRUST 1.0 elsewhere (Laske et al., 2013)). For oceans the map shows crustal thickness plus bathymetry; for continents — crustal thickness minus topography.

continental plate such as along the Pacific margin of South America, due to significant differences in density structure of oceanic and continental lithosphere caused by differences in crustal thicknesses (Figs. 2, 6), average crustal densities, and lithosphere buoyancies.

In case of continent–continent collision, it is also the heavier lithospheric plate that should subside. Given compositional differences in the structure of iron-depleted cratonic and fertile Phanerozoic lithospheric mantle, ancient lithosphere is lighter and thus more difficult to subduct (Sizova et al., 2010). In some rare cases, the presence of a subducting slab beneath modern collisional orogens is *not* imaged by geophysical data (e.g. the Caucasus, Sarker and Abers, 1998) or instead the presence of a delaminated lithospheric block (the Vrancea zone in the Carpathians, the Gibraltar arc in the Alboran sea) is proposed based on seismic and gravity data (Sperner et al., 2001; Molnar and Houseman, 2004; Lorinczi and Houseman, 2009; Levander et al., 2014). Similarly, lithosphere delamination has been proposed for other continent–continent collisional zones such as the southern Puna plateau of the Andes (Kay and Kay, 1993), Tibet (Turner et al., 1993; England and Molnar, 1997) and Himalaya (England and Houseman, 1989).

Plate boundary zones form only when continental plates are involved, and are mostly common when two continental plates collide (four examples are shown in Fig. 4). Series of subduction zones may be associated with broad zones of lithosphere deformation, such as in the Mediterranean region (Carminati et al., 2012; Zhu et al., 2012) and in the orogenic belt of the Central Asia (Sengör and Natal'in, 1996; Xiao et al., 2013), where seismic tomography images also the presence of paleoslabs in the upper mantle (Van der Voo et al., 1999a,b). Paleosubductions may also be responsible for significant seismic anisotropy with the dipping fast axis, such as observed in the upper mantle of central Europe (Babuska and Plomerova, 2006).

Topographic evolution during collision of lithospheric plates depends on the nature of the plates: oceanic or continental. When an oceanic plate is involved in plate collision, ocean trenches are formed on the side of the subducting oceanic plate (Fig. 2ab and examples in Fig. 4). Mantle melting in the wedge above the subducting slab, in the

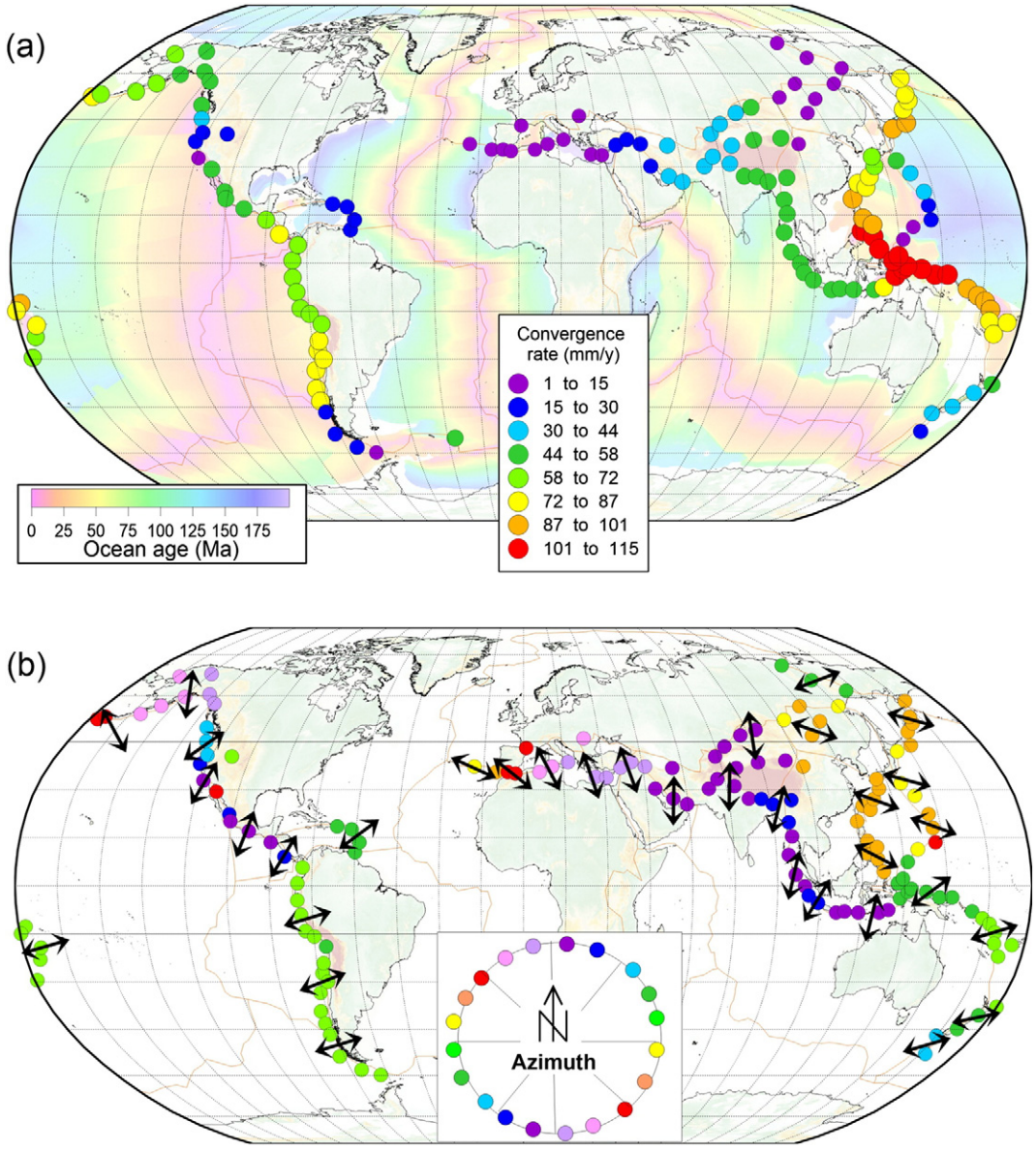

Fig. 7. Convergence rate (a) and direction (b) across different convergent margins for 140 locations shown by color dots (the values are based on the MORVEL plate velocity model, DeMets et al., 2010); (c) statistical distribution of convergence rate across the convergent margins of different types for locations shown by color dots in (a, b). Lines — best fit for Gaussian distribution. Convergence direction in (b) is shown both by color coding and by arrows.

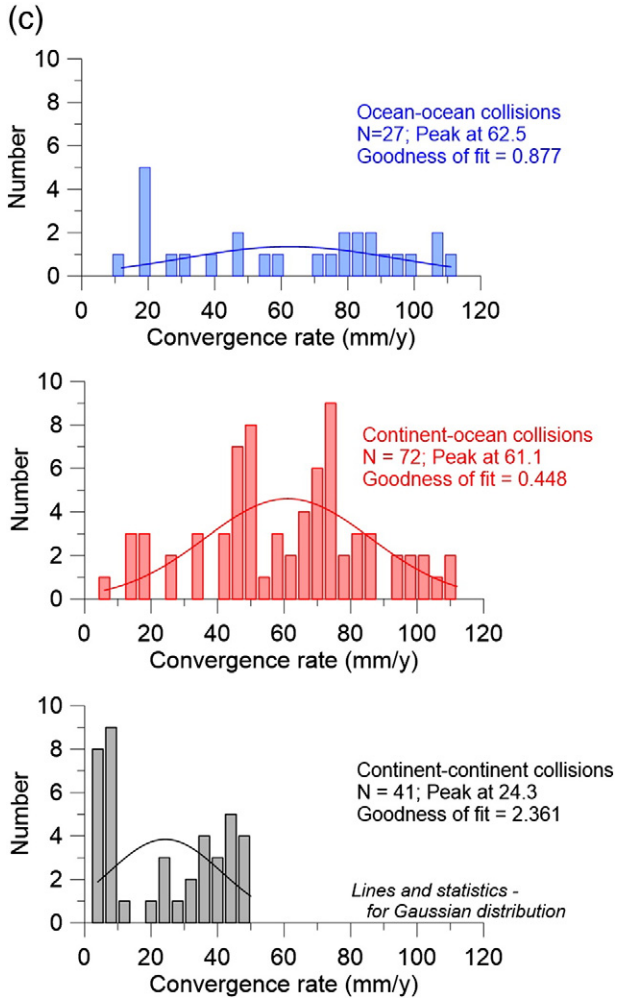

Fig. 7 (*continued*).

presence of water released by the downgoing slab, produces a chain of volcanoes (volcanic arc). This is the tectonic setting where most of the andesitic continental crust is thought to be generated (Kushiro, 1974), although the details of this process are still debated (Kay and Kay, 1993; Rudnick, 1995; Jagoutz and Behn, 2013).

Orogens form only when continental plates are involved. Basaltic magmas generated by mantle wedge melting pond at the crust–mantle boundary producing a high-velocity lower-crustal layer (magmatic underplating) observed in many modern and paleo-collisional settings, and similar processes in oceanic island arcs may be the primary mechanism for the production of continental crust (Thybo and Artemieva, 2013). Magma ascend through the crust in the form of sills and magmatic intrusions, the geometry of which is essentially controlled by crustal rheology (Gerya and Burg, 2007), increases crustal volume and leads to formation of crustal roots typical of the collisional orogens (Fischer, 2002; Artemieva and Meissner, 2012). In case of continent–continent collision, deep foreland basins are formed in front of mountain chains (Fig. 2c). The deepest known from seismic surveys is more than 8–10 km deep (e.g. the Caucasus foredeep, the Aquitaine basin along the northern edge of the Pyrenees) (ECORS Pyrenees Team, 1988; Artemieva and Thybo, 2013).

3. Convergence rate

We use the MORVEL plate velocity model (DeMets et al., 2010) to assess the convergence rate at ca. 300 locations along the convergent margins and to analyze if the convergence rate depends on the type of lithospheric plates involved in convergence (Fig. 7). The analysis indicates that usually the continent–continent convergent margins have a significantly smaller convergence rate than the margins where one of the plates is oceanic (Fig. 7c). The smallest values of convergence (<30 mm/y) are characteristic of broad plate boundary zones (Fig. 7a).

There are no systematic patterns when oceanic plates are involved into convergence. Statistical analysis demonstrates that a broad range of convergence rates is characteristic of both ocean–ocean and ocean–continent collisional settings. The peaks in the Gaussian distributions are at the same rate value (ca. 62 mm/y), which approximately corresponds to the median value of the convergence rate worldwide (Fig. 7c). The convergence rate appears to be controlled by (i) the lithospheric plate itself (plate size, lithosphere structure, including its rheology and thickness), (ii) the structure (size and lithosphere structure) and motion (direction and speed) of the adjacent plates, as well as (iii) by dynamics of the underlying mantle (direction of convective flow in the mantle, mantle viscosity, plumes, etc.).

It is, however, remarkable, that the oldest oceanic plate in the Pacific ocean has the smallest convergence rate. This observation may question the role of subduction pull in plate movement (Forsyth and Uyeda, 1975). Ideally subduction pull would be strongest for the oldest, coldest plates due to their strong temperature difference to the surrounding mantle. However, taking metamorphic reactions in the downgoing plate into account, we find that the extra negative buoyancy force on the old plates may lose its importance from the depths where main metamorphic reactions take place, and where younger plates will gain density contrast with the surrounding mantle similar to the old plates.

4. Seismicity at convergent margins

Subducting lithospheric slabs is the cause of seismicity at convergent margins (Fig. 8ab). In contrast to the transform and constructive margins where seismicity is generally low- and intermediate-magnitude, the convergent margins generate the strongest earthquakes. With very few exceptions, high-magnitude ($M > 8.0$) earthquakes all require the presence of an oceanic plate (Fig. 8a), and such strong earthquakes can rarely be generated at continent–continent collisions, where seismic magnitude usually is less than 7.5–7.8. The strongest earthquakes seem to be associated with the continent–ocean collision zones.

Continent–continent collisions are manifested by broad zones of shallow (<200 km) seismicity which marks plate boundary zones. Termination of seismicity below ca. 200 km depth (Fig. 9) may mark the depth extent of the continental lithosphere involved in continent–continent collisions. However, most seismicity is restricted to the crust, the number of events at the sub-Moho depth is small, and, in contrast to oceanic subduction zones, they rarely form linear belts of progressive deepening of epicenters with distance from the collision plane (Fig. 8b).

The only exceptions are the Zagros mountains in southern Iran and the Pamir mountains at the western end of the Himalayas, where intermediate depth seismicity is common. The presence of a subducting slab beneath the Zagros orogen, which formed in association with the closure of the Tethys ocean during the collision of Eurasia and Arabia, has been imaged by seismic tomography (Alinaghi et al., 2007; Agard et al., 2011); the presence of two ophiolite belts parallel to the strike of the orogen (Moghadam and Stern, 2011) suggests oceanic origin of the slab. The presence of the downgoing slab beneath the Pamir has been proposed by a number of studies; it generates seismicity down to ca. 350 km depth and has a steep dip of ca. 70–90°. However, the origin of this slab (subduction of the Eurasian plate beneath the Pamir (Burtman and Molnar, 1993) or subduction of the detached Indian oceanic plate beneath the Hindu Kush (Koulakov and Sobolev, 2006)) is still a subject of debate. The pattern of seismicity in the Pamir is alike seismicity in the Vrancea zone of the Carpathians, where a seismogenic body with ca. 30 km × 70 km lateral extent dips at a near-vertical

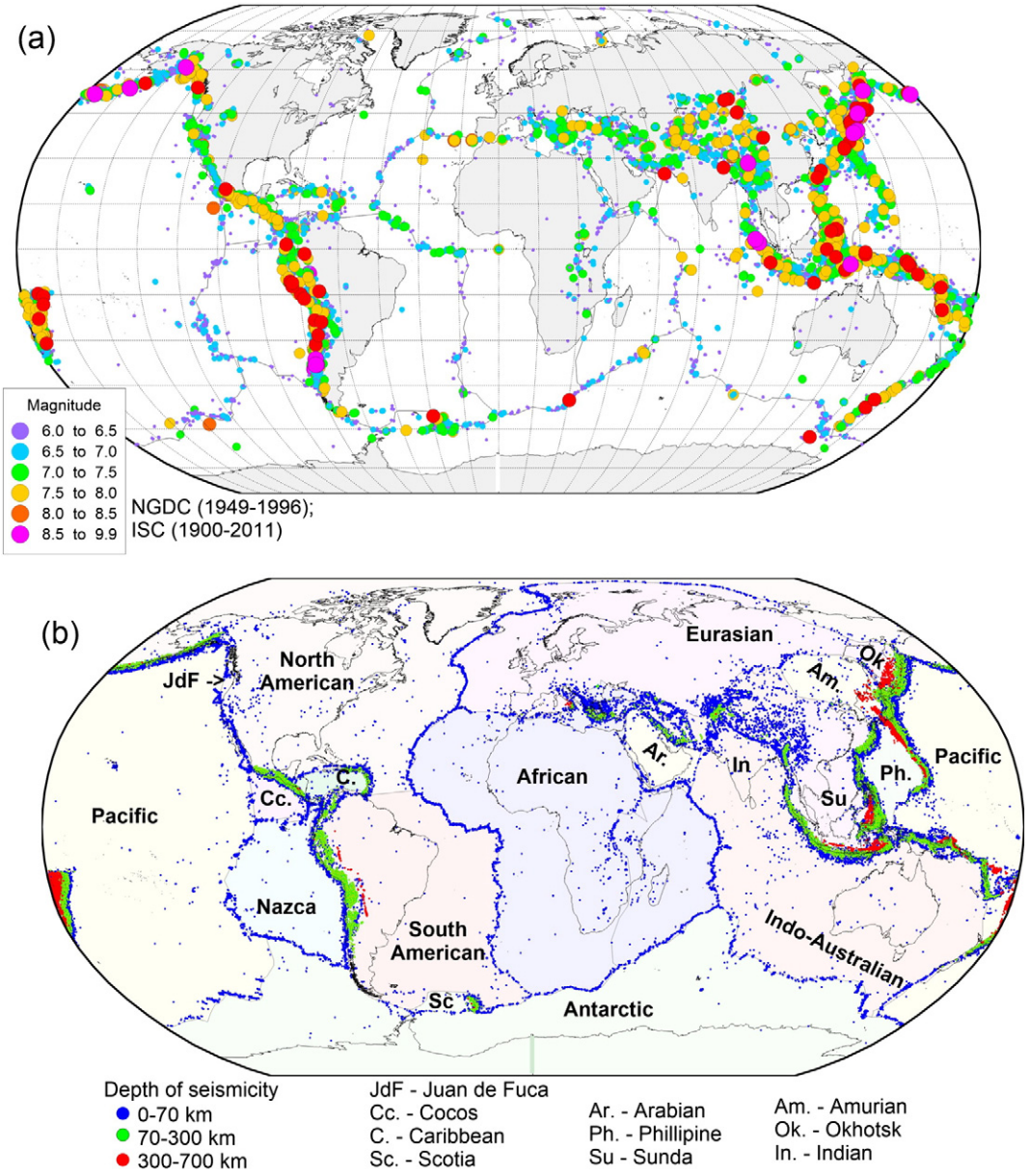

Fig. 8. Global distribution of seismicity: (a) with M > 6.0, color-coded according to magnitude (based on NGDC data for 1949–1996 and ISC-GEM data for 1900–2011, Storchak et al., 2013); (b) by depth (dots of three colors) with indication of major plates.

angle down to ca. 200 km depth (Fig. 10a), and a high-velocity body extending down to ca. 350 km depth has been imaged by seismic tomography (Wortel and Spakman, 2000; Bokelmann and Rodler, 2014). Similar to the Pamir, the geodynamic origin of this body is debated, and various models involving either descending relic oceanic lithosphere of the Tethys ocean (Csontos, 1995; Wortel and Spakman, 2000) or continental lithosphere (attached, detached or delaminated) (Knapp et al., 2005; Lorinczi and Houseman, 2009) have been proposed. Our analysis of seismicity patterns at different types of convergent margins (Fig. 10bc) suggests that the presence of an oceanic plate is a precondition for generating intermediate and deep seismicity. We therefore favor oceanic origin of subducting slabs beneath the Zagros, the Pamir, and the Vrancea zone.

Deep seismicity (>300 km) requires the involvement of an oceanic plate, and from the first glimpse there is no principal difference between the depth distribution of seismicity at ocean–ocean and ocean–continent convergent margins (Fig. 9b). Characteristic of a subducting oceanic slab is zonal pattern of the epicentral depths, which deepen away from the plate boundary. Such pattern is clearly seen for the Andes and for the subduction zones along the western margin of the Pacific ocean (Fig. 8b).

A detailed analysis of depth distribution of seismicity in subducting oceanic slabs shows a remarkable pattern (Fig. 10), with a sharp distinction between ocean–ocean and continent–ocean convergent margins. When two oceanic plates collide, the downgoing slab preserves its integrity down to the mantle transition zone and, in some cases, even across the transition zone (Figs. 4 and 10b). In sharp contrast, oceanic slab subducting beneath a continent is not seismogenic at depths between 200–300 km and 500–600 km (Fig. 10c). The dip of subduction is usually different in the upper and lower parts; it becomes significantly steeper within or below the transition zone, where it becomes near-vertical.

5. Dip angle of subduction

Numerous studies that tried to link the dip angle of subduction to various parameters have demonstrated that there is no unique

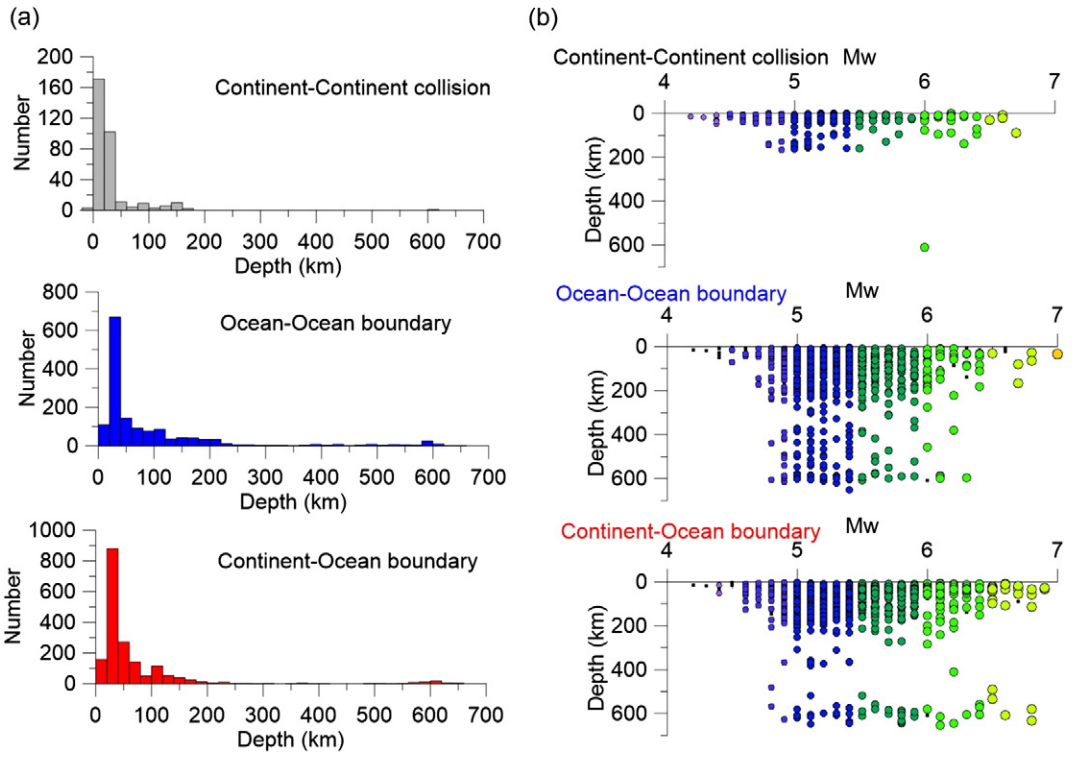

Fig. 9. Seismicity distribution with depth (based on ISC-GEM catalogue, Storchak et al., 2013). Seismic events calculated within 200 km-wide corridors along the profiles in Figs. 3 and 4.

dependence and a number of factors may control subduction dip (Hayes et al., 2012). The most important are the relative velocity of the converging plates and the negative buoyancy force of the descending slab (Yokokura, 1981); although the overriding plate may have an important feedback on the dynamics of subduction (Capitanio et al., 2010). Numerical analysis with account for the thermal structure of subducting plates with finite length has shown that long slabs that have penetrated the mantle transition zone are unstable and rotate towards steeper dip angles (Hsui et al., 1990). It is consistent with the pattern observed in Fig. 10c.

Our analysis indicates that, in case of continent–ocean subduction, there is no correlation between the dip angle, on the one side, and the age of subducting oceanic slab (hence, its thermal structure) and the convergence rate, on the other side (Fig. 11). We also do not find any correlation between the dips of subduction at the shallow (sub-Moho) depth and below a 200 km depth, although with no exception the dip increases from shallow mantle to the transition zone (Fig. 11a).

Although our analysis includes only 4 profiles across ocean–ocean convergence (Figs. 3, 4), the results demonstrate a strong control of the thermal structure of the descending slab (controlled by the age of subducting oceanic plate) and the relative velocity of the converging oceanic plates on subduction dip:

- old oceanic plates with thick lithosphere subduct at more shallow angle than young oceanic plates (Fig. 11b) which may be contrary to expectations (e.g. Uyeda and Kanamori, 1979);
- oceanic plates with high convergence rate produce steep dipping slabs (Fig. 11c); and
- at very high convergence rate, at depths below ca. 500 km the downgoing slab rotates towards a near-vertical dip angle (Fig. 11d).

6. Gravity anomalies

We present three maps for gravity anomalies (Fig. 12) constrained by the high-resolution EGM2008 global gravity model (Pavlis et al., 2012): free-air anomaly, horizontal gradient of the free-air anomaly, and Bouguer anomaly. The maps and profiles illustrate the fundamental difference between the density structure of continents with near-zero Bouguer anomalies (except for orogenic environments) and of oceans with large positive Bouguer anomalies.

Strong free-air anomalies of, in pairs, positive and negative signs demonstrate that local isostasy is not satisfied at the convergent margins. Ocean trenches at ocean–ocean and continent–ocean convergent margins are usually marked by a strong peak of positive free air anomalies (+50 + 200 mGal), with a narrow belt of strong negative anomalies (−100–300 mGal) parallel to the trench on the side of the downgoing slab (Figs. 4, 12a). In collisional orogens, the strongest anomalies are localized to the marginal parts of plate boundary zones, where subducting slabs are present. Positive free-air anomalies in zones of continent–continent collision (Fig. 4) imply that these plate boundary zones are undercompensated and will sink if external stress is removed, in particular along the Himalayan to Alpine orogen that formed after closure of the Tethys ocean. An exception is the Tibet, where free-air anomalies are close to zero. It suggests that the Tibetan plateau is nearly compensated and a strong density anomaly should be present within the lithospheric mantle, giving support to the hypothesis of crustal/lithospheric doubling below Tibet.

The map of horizontal gradient of the free-air anomaly (Fig. 12b) shows mainly anomalies at the active (destructive and constructive) plate boundaries, with the strongest anomalies across the convergent margins, whereas the constructive plate boundaries (along mid-ocean ridges) are observed as weak anomalies.

The maximal amplitude of gradient of free-air anomalies is across convergent margins with involvement of oceanic plates. In continent–ocean collisions, the zone of high gradient free-air anomalies is usually broader than in case of ocean–ocean convergence, and it is very wide in plate boundary zones. A number of paleoconvergent margins (such as the Urals) are clearly marked by a large gradient of free-air anomalies. In other places, however, similar linear belts of large gravity gradients are associated not with convergent margins but with magmatic intrusions (hotspot tracks, the East African Rift). There is no evidence for a

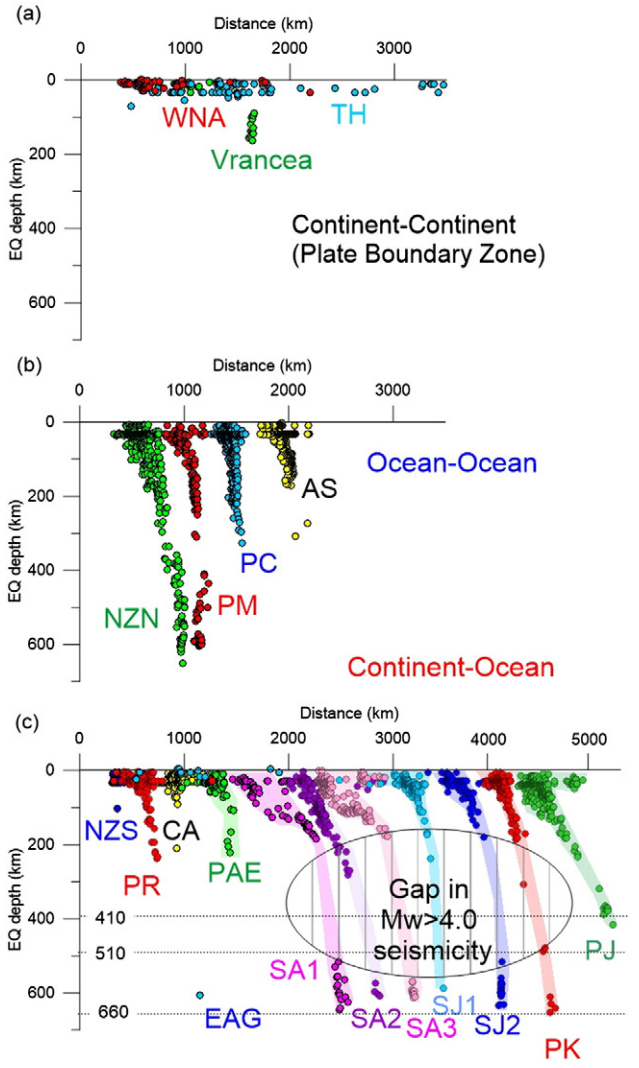

Fig. 10. Stacked seismicity distribution with depth (within 200 km-wide corridors along the profiles in Fig. 3, based on ISC-GEM catalogue, Storchak et al., 2013). Data for individual profiles is shifted to simplify visualization. For profile names and locations see Fig. 3. Vertical and horizontal scales are the same for all three types of convergent margins. The patterns of seismicity distribution with depth are significantly different for three types of convergent margins.

hotspot track around Iceland, and we speculate that Iceland may be the birthplace of a new mantle plume, if it exists. In contrast to convergent margins and hotspot tracks, volcanic passive margins and mid-ocean ridges have very weak anomalies in free-air gravity gradient.

The map of Bouguer gravity anomalies (Fig. 12c) primarily shows the difference between the low-density continental and the high-density oceanic lithosphere. Within the oceans, extremely high Bouguer anomalies coincide with old (roughly >50 Ma) oceans and indicate the presence of high-density lithosphere, whereas the positive anomalies are substantially smaller in regions with young oceanic crust (around mid-ocean ridges) and around magmatic regions (e.g. volcanic margins and hotspot tracks).

Similarly, at the convergent margins, strong positive Bouguer gravity anomalies are associated with old oceanic lithosphere and smaller positive anomalies are associated with volcanic arcs, whereas negative anomalies are associated with continental orogens, indicative of crustal roots. The convergence zone at Tibet has a strong negative anomaly over a large area, which provides further evidence for the crustal or lithospheric stacking of the Eurasian and Indian plates. However, palaeo-orogens do not exhibit strong Bouguer anomalies.

7. Thermal structure across the convergent margins

As discussed above, we find that the thermal structure of the downgoing slab may have strong effect on the subduction dip (Fig. 11). We try to address the thermal structure of convergent margins by analyzing data on surface heat flow (Fig. 13) and upper mantle seismic shear-wave velocity structure (Fig. 14).

Surface heat flow does not show systematic variations across the convergent margins (Figs. 4 and 13), although some general patterns have been recognized for the Circum-Pacific subduction zones (Currie and Hyndman, 2006; Wada and Wang, 2009). There is a general tendency for higher heat flow above or around volcanic arcs and in the back-arc basins (Fig. 4). Low heat flow is measured in some young continental orogens (e.g. Tibet). However, in these regions heat flow anomaly in the mantle may be too young for the thermal perturbation to reach the surface and to be reflected in the present surface heat flow.

The problem in recognizing regional patterns, especially across oceanic margins, may largely be due to strong heterogeneity of measured heat flow values where the measurements may be strongly affected by factors that are not readily controllable, such as hydrothermal circulation in shallow crustal layers (in particular in the oceanic environment, including marine sediments), local magmatic activity associated with volcanic arcs and magmatic intrusions into the crust, crustal faulting common in regions of active tectonics, and horizontal heat transfer in regions with a high contrast in thermal properties (which one would expect at convergent margins). Note that in many convergent settings the number of heat flow measurements is low (Fig. 13c), which further complicates interpretations and recognition of patterns for convergent margins of different types.

The analysis of the upper mantle velocity structure shows that at depth <100 km, mid-ocean ridges with partial melting in the shallow mantle dominate the pattern as linear low-velocity anomalies (Fig. 14a). However, a tendency for low upper mantle velocity is also found in the distributed continental convergence zones, e.g. Tibet, the Himalayan to Alpine orogens, and western North America. Very strong gradient in Vs anomalies at 75–125 km depth is typical of ocean–ocean and, in some cases, continent–ocean convergent margins; these anomalies are associated with mantle wedge melting. In areas of continent–continent collision (e.g. Tibet), Vs anomalies at a 75 km depth may be associated with deep crustal roots. Deeper in the upper mantle, at 175 km depth, strong low-velocity anomalies are no longer observed across the convergent margins, thus indicating that shallow melting within the mantle wedge is characteristic of these tectonic settings (Fig. 14c). At these depths, it appears that the main anomalies in seismic velocity are related to the roots of cratonic lithosphere (Artemieva and Mooney, 2001).

8. Seismic images of convergent margins

A large variety of seismic data from presently active convergent margins provide a wealth of information on their crustal and upper mantle structure. The literature is so comprehensive that we limit ourselves to mentioning only a few publications from the various tectonic settings discussed in this paper. We refer the reader to Table 2 for a more comprehensive overview of seismic models of convergent margins.

Type examples of an ocean–ocean convergent margin that were imaged seismically include the Tonga–Kermadec subduction zone (Contreras-Reyes et al., 2011; Stratford et al., 2015) and the North Island of New Zealand (Reyners et al., 2006; Stern et al., 2015). A recent controlled-source seismic experiment provided a high-resolution image of the base of a subducting oceanic plate which is dipping at ca. 15 beneath North Island of New Zealand (Stern et al., 2015). Seismic data show a sharp, less than 1 km thick, seismic boundary with a ca. 8% decrease in Vp velocity that is parallel to the top of the subducting plate. The presence of a parallel reflection located ca. 10 km deeper

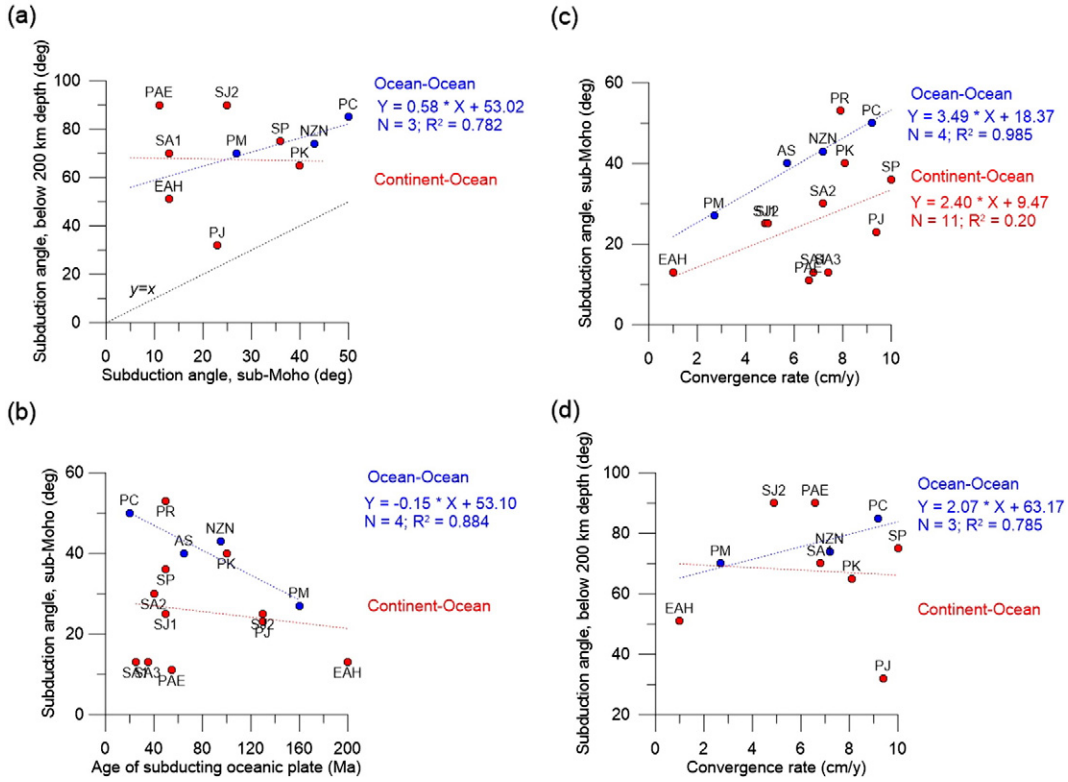

Fig. 11. Subduction dip at different convergent margins (see Fig. 3 for profile names and locations; Table 1 and Fig. 4 for details). Correlations between: (a) slab dip angle at sub-Moho depth and dip angle at depth below ca. 200 km; (b) age of subducting oceanic plate and slab dip angle at sub-Moho depth; (c) convergence rate and slab dip angle at sub-Moho depth; (d) convergence rate and dip angle at depth below ca. 200 km. Blue colors — for ocean–ocean convergence; red colors — for continent–ocean convergence; labels refer to profile codes in Figs. 3–4 and Table 1. Red and blue lines — bet linear fit; R^2 is coefficient of determination. Strong correlations are observed for ocean–ocean convergence margins, but no correlations exist when continental plates are involved in convergence.

has been interpreted as evidence for a low-viscosity channel along the base of the lithospheric plate. This channel formed by partial melts or fluids acts as the decoupling zone between the lithosphere and the convecting mantle.

Seismic studies of the Kuril arc in northern Japan show clearly a subducting slab, above which the volcanic arc develops (Nakanishi et al., 2009). The magmatic arc is divided into forearc and accretionary complex above the new magmatic crystalline crust, which has a distinctly different upper crust of a relatively low velocity and a lower crust with a very high velocity. It is believed that such magmatic arc may be the primary origin of continental crust if tectonic processes may separate the upper from the lower crust (e.g. Taylor, 1967; Tatsumi, 2005). However, the process is not yet fully understood, because hydrous melts produced by peridotite melting in mantle wedge are basaltic, and different mechanisms were proposed for how they may acquire andesitic composition to produce continental crust (Kay and Kay, 1993; Rudnick, 1995; Jagoutz and Behn, 2013).

Continent–ocean convergent margins have been extensively imaged along the western coast of the Americas. In Chile, a series of normal-incidence reflection and wide-angle reflection/refraction images of the convergent margin have been observed (e.g. ANCORP Working Group, 1999; Oncken et al., 2003), supplemented by receiver function (Yuan et al., 2000) and seismic tomography of the upper mantle (Schurr et al., 2006). In North America, images of the convergent margin include a seismic refraction model (Trehu et al., 1994), a combined normal-incidence reflection and wide-angle reflection/refraction model around the Vancouver Island (Hyndman et al., 1990; Calvert, 1996), and a recent POLARIS seismic project across the Cascadia subduction zone which shows the presence of an eastwards dipping low-Vs anomalous body below the Vancouver Island (Nicholson et al., 2005). Some of the most recent images of continent–ocean subduction complexes have been obtained along the Sunda-Java convergent margin in Indonesia, with significant variations in subduction style along the margin (e.g. Lüschen et al., 2011; Shulgin et al., 2011).

Continent–continent convergence systems are particularly numerous in Eurasia. Controlled source seismology provided images across the Pyrenean system (e.g. ECORS Pyrenees Team, 1988; Mezcua and Rueda, 1997) and the Alps (Brückl et al., 2007), whereas seismic tomography and receiver functions have been recently intensively applied along the whole post-Tethys collisional belt (e.g. Kind et al., 2002; Lippitsch et al., 2003; Souriau et al., 2008; Zhang et al., 2012). The broad zone of continental deformation in the Tibet-Himalayas region has been intensively studied by a large number of international experiments and we refer the reader to the corresponding publications (e.g. Brown et al., 1996; Kind et al., 2002; Tilmann et al., 2003; Wittlinger et al., 2004; Yao et al., 2006).

Geophysical imaging in a number of ancient continental terranes, that have been tectonically quiet since the late Archaean or Proterozoic, has identified structures in the upper mantle that are similar to the images of presently active subduction settings. These images provide constraints on the time when plate tectonics begun. The oldest imaged paleosubduction is in the eastern Canadian shield, where a clear dipping seismic reflection is observed over a depth range of approximately 30 km from the Moho into the upper mantle (Calvert et al., 1995). Given a strong contrast in crustal structure around the same location combined with geochronological dating of shear zones and terranes, this image has been interpreted as evidence for continent–continent collision at 2.69 Ga. Similar image, including a 10 km offset on the

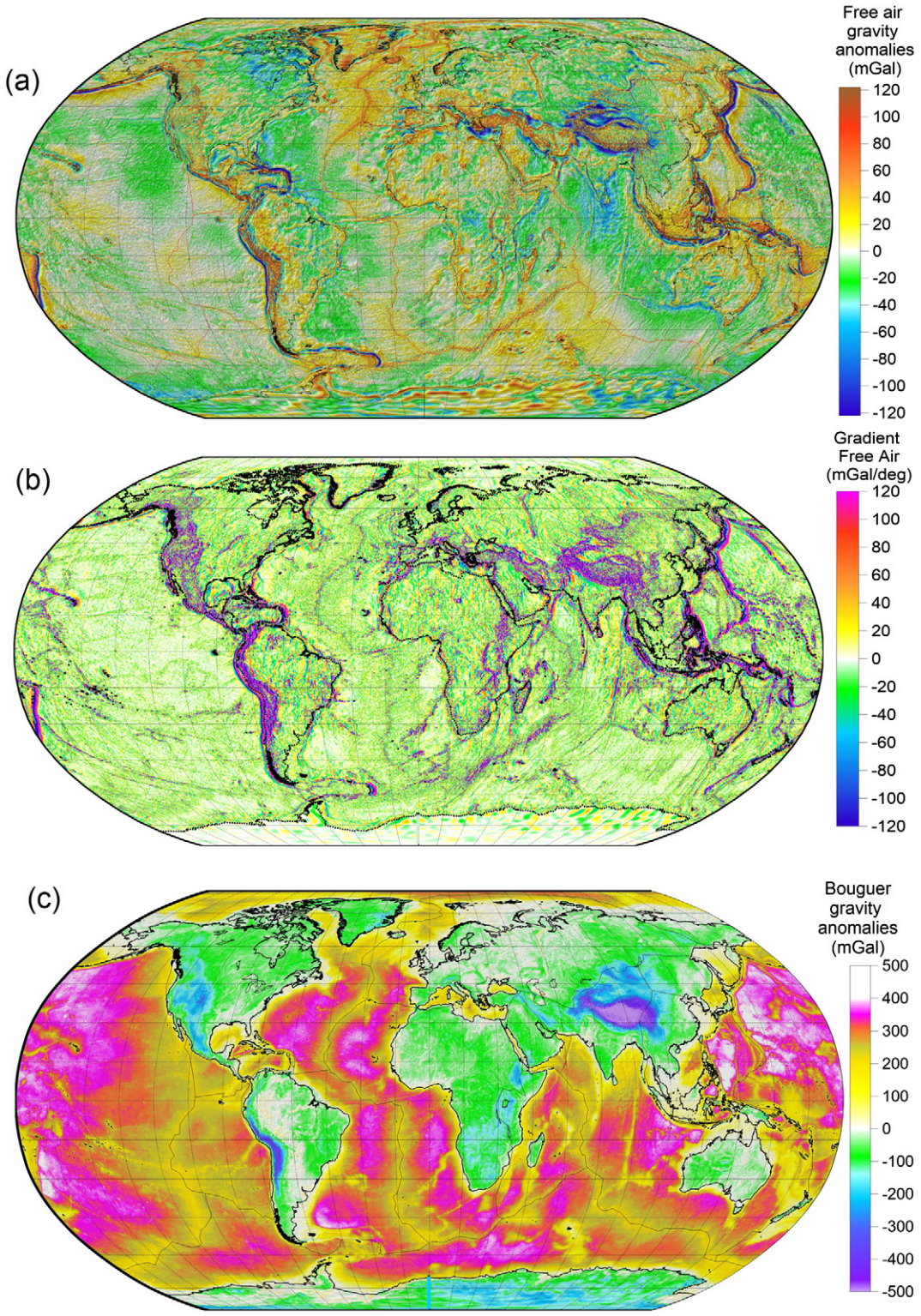

Fig. 12. Gravity anomalies (based on EGM2008, Pavlis et al., 2012): (a) free air anomalies; (b) horizontal gradient of free air gravity anomalies; (c) Bouguer gravity anomalies (reduction is based assuming density of 2670 kg/m^3 for topography, 1050 kg/m^3 for water, and 919 kg/m^3 for ice).

Moho, was earlier obtained for the Baltic Shield and interpreted as a 1.89 Ga old continental collision belt (BABEL Working Group, 1990). Further south in the Baltic Shield, coincident wide-angle seismic data show that another dipping mantle reflector, related to a 1.86 Ga continental collision, is associated with a pronounced change in seismic velocity from ca. 7.9 to 8.2 km/s thus providing a clear indication for collision between two plates of different origins (Abramovitz et al., 1997). Proterozoic collision has been also documented in northwestern Canada where a dipping mantle reflection was imaged down to ca. 80 km depth (Cook et al., 1997) and by inferred interpolation with a receiver function image it has been extended to ca. 200 km depth (Bostock, 1999).

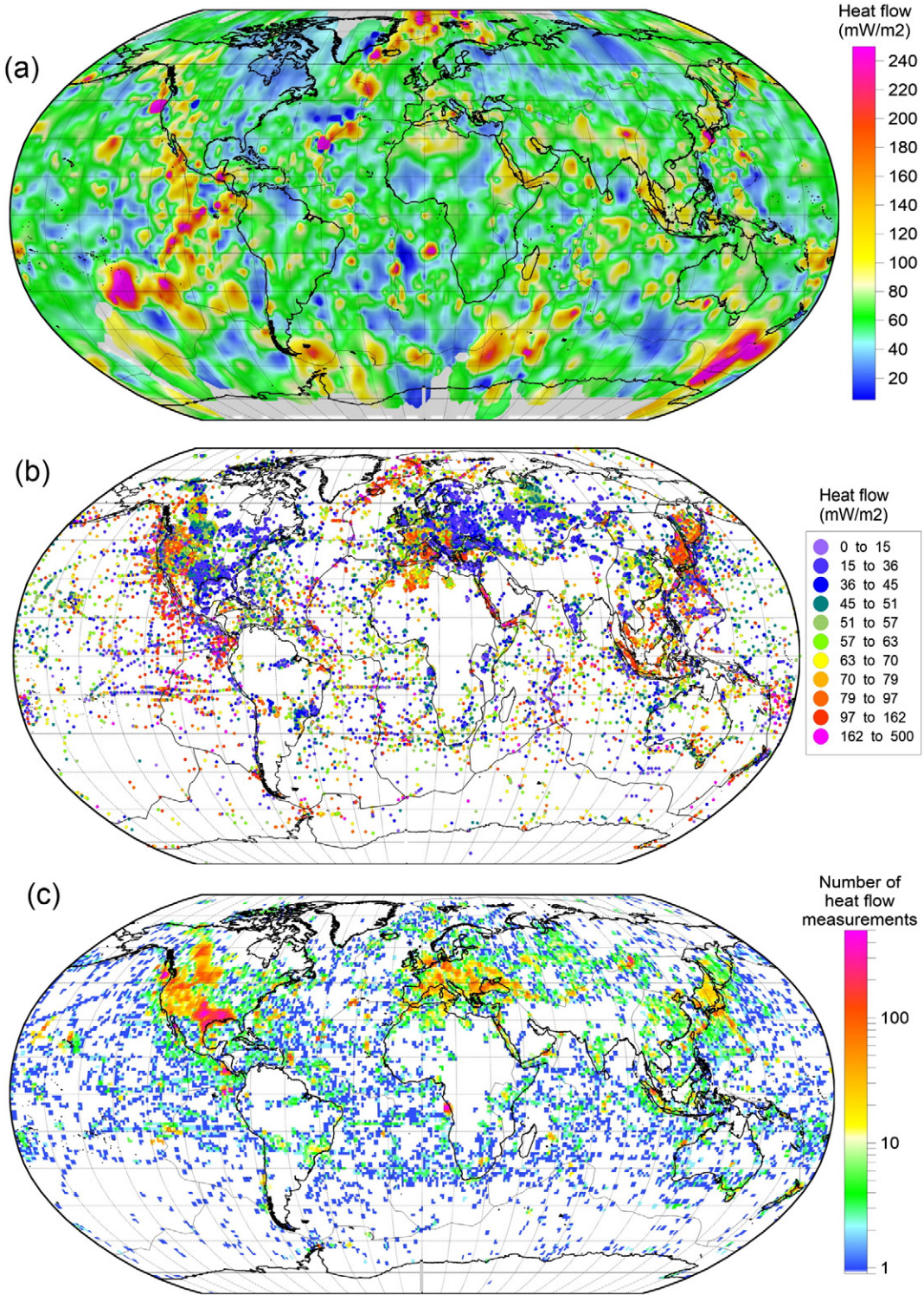

Fig. 13. Surface heat flow (based on compilation of IHFC, 2011): (a) interpolation (with a 20 deg radius) based on point heat flow measurements on continents and in oceans (b); (c) density of heat flow measurements counted for $1^\circ \times 1^\circ$ cells.

Younger orogenic events related to Sveconorwegian (Grenvillian) collision have been recognized by reflection seismic observation of dipping mantle reflections in the North Sea region in Europe (Lie et al., 1990). In two places in northern Europe, spectacular Caledonian structures have been imaged in the upper mantle (Warner et al., 1996; MONA LISA Working Group, 1997). A significant wide-angle observation of variation in seismic velocity across the dipping mantle reflectors was observed at the MONA LISA profiles, as well as indication for anisotropy with the fast axis along a dipping slab (Abramovitz and Thybo, 2000). Wide-angle seismic and teleseismic data provide evidence for paleosubduction at the transition between the Precambrian East-European Craton and Phanerozoic Europe (e.g. Zielhuis and Nolet, 1994; Grad et al., 2002; Shomali et al., 2006).

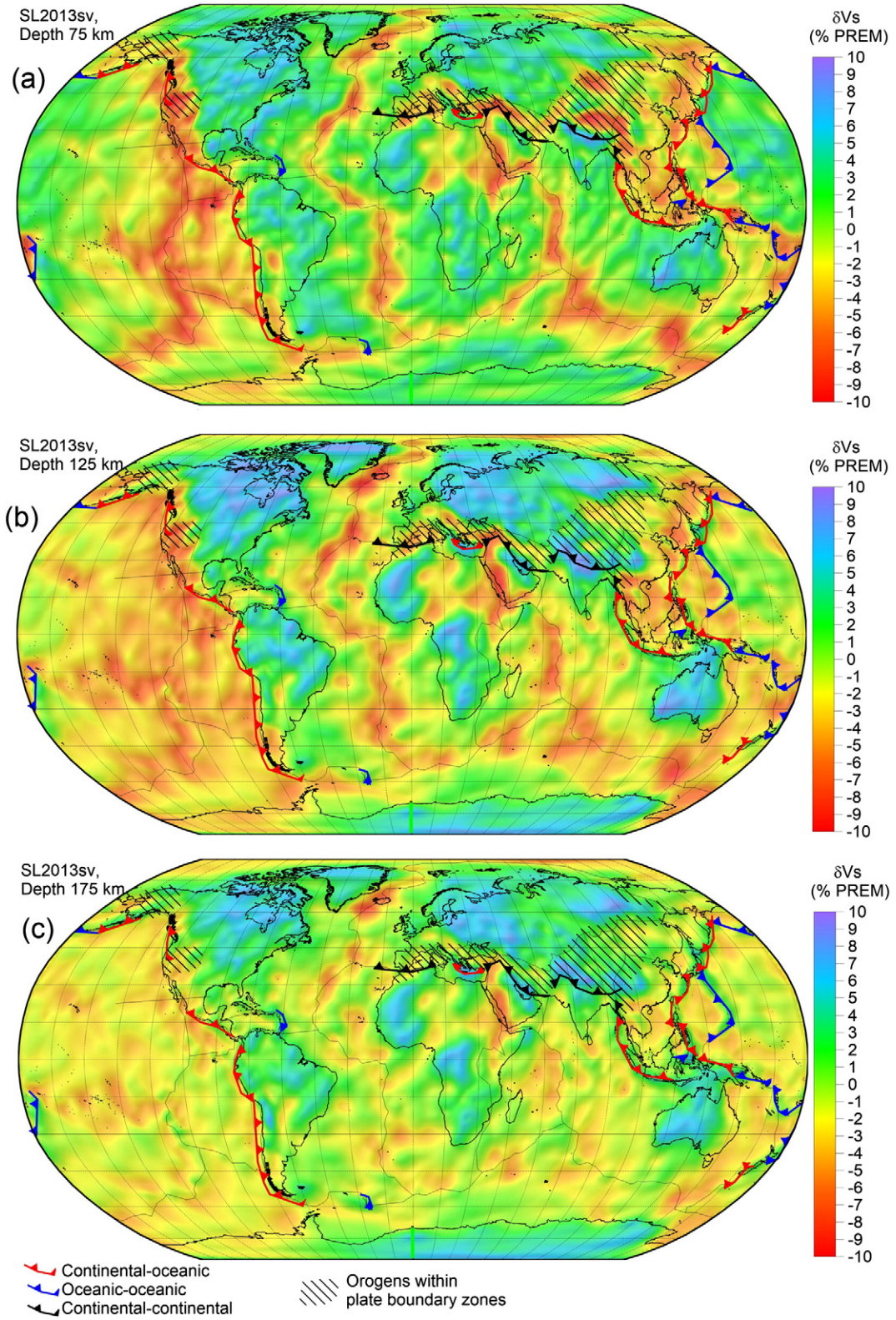

Fig. 14. Relative perturbations (with respect to PREM) of Vs seismic velocity in the upper mantle at depths of 75 km (a), 125 km (b), and 175 km (c) (based on surface wave tomography model SL2013sv, Schaeffer and Lebedev, 2013).

9. Conclusions

We have presented a series of maps and profiles based on geophysical (gravity, seismic, thermal) data in order to illustrate the effects of the plate tectonic processes at convergent margins on the crustal and upper mantle structure, seismicity, and geometry of subducting slab. Based on the presented data we conclude:

- Plate convergence rate depends on the type of convergent margin, but does not show any systematic patterns. Convergence rate is

significantly larger when one of the plates is oceanic, and the smallest values of convergence rate are characteristic of the plate boundary zones between two colliding continental plates. Unexpectedly, the oldest oceanic plate in the Pacific ocean has the smallest convergence rate, which may indicate that the temperature of the subducting slab has less importance for the downward forces than the density contrasts that develop due to metamorphic reactions in the downgoing slab.

- Our analysis of seismicity patterns reveals that, with very few exceptions, high-magnitude ($M > 8.0$) earthquakes all require the presence of an oceanic plate, and the strongest earthquakes seem to be restricted to the continent–ocean collision zones. The results also indicate that the presence of an oceanic plate is a pre-condition for generating intermediate (70–300 km) and deep (300–700 km) seismicity along the convergent margins. Subducting oceanic slabs are seismogenic to depths of around 700 km, and oceanic slabs subducting beneath a continent are not seismogenic at depths between ca. 250 km and 500 km. In case of continent–continent collision, the seismogenic zone terminates at ca. 200 km depth. Based on this observation, we propose oceanic origin of subducting slabs beneath the Zagros, the Pamir, and the Vrancea zone, where seismicity extends below a 200 km depth.
- Our analysis of subducting slab dip angle shows different patterns for different types of convergent margins. For continent–ocean subduction, there is no correlation between the dip angle and the age (thermal structure) of the subducting oceanic slab, nor the convergence rate. We find, however, clear trends for ocean–ocean subductions. Old oceanic plates with thick lithosphere subduct at shallower angles than young oceanic plates. High convergence rate of oceanic plates leads to steeply dipping slabs, and at very high convergence rate, the downgoing slab rotates towards a near-vertical dip angle at depths below ca. 500 km.
- Strong free-air gravity anomalies of positive and negative signs demonstrate that local isostasy is not satisfied at the convergent margins. However, there may be a near-isostatic equilibrium in large distributed deformation zones, such as Tibet.
- Low seismic velocities in the upper mantle beneath convergent margins down to depths of 150 km may be related to mantle wedge melting. The termination of the low velocity anomalies at a 175 km depth indicates that melting within the mantle wedge is confined to shallower levels.

Acknowledgments

IA gratefully acknowledges DFF-FNU grant 1323-00053. The study has been inspired by the International Symposium on Convergent Margins (Trabzon, Turkey, 2014) organized by Dr. Y. Eyuboglu.

References

Abramovitz, T., Thybo, H., 2000. Seismic images of Caledonian, lithosphere-scale collision structures in the southeastern North Sea along MONA LISA Profile 2. Tectonophysics 317, 27–54.

Abramovitz, T., Berthelsen, A., Thybo, H., 1997. Proterozoic sutures and terranes in the southeastern Baltic Shield interpreted from BABEL deep seismic data. Tectonophysics 270, 259–277.

Agard, P., Omrani, J., Jolivet, L., Whitechurch, H., Vrielynck, B., Spakman, W., Moni_e, P., Meyer, B., Wortel, R., 2011. Zagros orogeny: a subduction-dominated process. Geological Magazine 148, 692–725.

Aitchison, J., Clarke, G., Meffre, S., Cluzel, D., 1995. Eocene arc–continent collision in New Caledonia and implications for regional southwest Pacific tectonic evolution. Geology 23, 161–164.

Alinaghi, A., Koulakov, I., Thybo, H., 2007. Seismic tomographic imaging of P- and S-waves velocity perturbations in the upper mantle beneath Iran. Geophysical Journal International 169, 1089–1102.

Amante, C., Eakins, B.W., 2009. ETOPO1 1 arc-minute global relief model: procedures, data sources and analysis. NOAA Technical Memorandum NESDIS NGDC-24. National Geophysical Data Center, NOAA. http://dx.doi.org/10.7289/V5C8276M.

ANCORP Working Group, 1999. Seismic reflection image revealing offset of Andean subduction-zone earthquake locations into oceanic mantle. Nature 397, 341–344.

Artemieva, I.M., Meissner, R., 2012. Crustal thickness controlled by plate tectonics: a review of crust–mantle interaction processes illustrated by European examples. Tectonophysics 519, 3–34.

Artemieva, I.M., Mooney, W.D., 2001. Thermal thickness and evolution of Precambrian lithosphere: a global study. Journal of Geophysical Research 106, 16387–16414.

Artemieva, I.M., Thybo, H., 2013. EUNAseis: a seismic model for Moho and crustal structure in Europe, Greenland, and the North Atlantic region. Tectonophysics 609, 97–153.

Audet, P., Bostock, M.G., Christensen, N.I., Peacock, S.M., 2009. Seismic evidence for overpressured subducted oceanic crust and megathrust fault sealing. Nature 457, 76–78.

BABEL Working Group, 1990. Evidence for early Proterozoic plate tectonics from seismic reflection profiles in the Baltic Shield. Nature 348, 34–38.

Babuska, V., Plomerova, J., 2006. European mantle lithosphere assembled from rigid microplates with inherited seismic anisotropy. Physics of the Earth and Planetary Interiors 158, 264–280.

Bokelmann, G., Rodler, F.A., 2014. Nature of the Vrancea seismic zone (Eastern Carpathians) — new constraints from dispersion of first-arriving P-waves. Earth and Planetary Science Letters 390, 59–68.

Bostock, M.G., 1999. Seismic imaging of lithospheric discontinuities and continental evolution. Lithos 48, 1–16.

Bostock, M.G., 2013. The Moho in subduction zones. Tectonophysics 609, 547–557.

Brocher, T.M., Parsons, T., Tréhu, A.M., Snelson, C.M., Fisher, M.A., 2003. Seismic evidence for widespread serpentinized forearc upper mantle along the Cascadia margin. Geology 31, 267–270.

Brown, L., Zhao, W., Nelson, K., et al., 1996. Bright spots, structure, and magmatism in Southern Tibet from INDEPTH seismic reflection profiling. Science 274 (5293), 1688–1690.

Brückl, E., Bleibinhaus, F., Gosar, A., Grad, M., Guterch, A., Hrubcova, P., Keller, G.R., Majdanski, M., Sumanovac, F., Tiira, T., Yliniemi, J., Hegedus, E., Thybo, H., 2007. Crustal structure due to collisional and escape tectonics in the Eastern Alps region based on profiles Alp01 and Alp02 from the ALP 2002 seismic experiment. Journal of Geophysical Research - Solid Earth 112. http://dx.doi.org/10.1029/2006JB004687.

Burtman, V.S., Molnar, P., 1993. Geological and geophysical evidence for deep subduction of continental crust beneath the Pamir. Geological Society of America 281 (85 pp.).

Calvert, A.J., 1996. Seismic reflection constraints on imbrication and underplating of the northern Cascadia convergent margin. Canadian Journal of Earth Sciences 33, 1294–1307.

Calvert, A.J., Sawyer, E.W., Davis, W.J., Ludden, J.N., 1995. Archaean subduction inferred from seismic images of a mantle suture in the Superior Province. Nature (London) 375, 670–674.

Calvert, A.J., Klemperer, S.L., Takahashi, N., et al., 2008. Three-dimensional crustal structure of the Mariana island arc from seismic tomography. Journal of Geophysical Research 113 (B1).

Capitanio, F.A., Stegman, D.R., Moresi, L.N., Sharples, W., 2010. Upper plate controls on deep subduction, trench migrations and deformations at convergent margins. Tectonophysics 483, 80–92.

Carminati, E., Lustrino, M., Doglioni, C., 2012. Geodynamic evolution of the central and western Mediterranean: tectonics vs. igneous petrology constraints. Tectonophysics 579, 173–192.

Cherepanova, Yu., Artemieva, I.M., Thybo, H., Chemia, Z., 2013. Crustal structure of the Siberian Craton and the West Siberian Basin: an appraisal of existing seismic data. Tectonophysics 609, 154–183.

Chou, H.C., Kuo, B.Y., Chiao, L.Y., Zhao, D., Hung, S.H., 2009. Tomography of the westernmost Ryukyu subduction zone and the serpentinization of the fore-arc mantle. Journal of Geophysical Research: Solid Earth (1978–2012) 114.

Contreras-Reyes, E., Grevemeyer, I., Flueh, E.R., Reichert, C., 2008. Upper lithospheric structure of the subduction zone offshore of southern Arauco peninsula, Chile, at similar to 38 degrees S. Journal of Geophysical Research 113 (B7). http://dx.doi.org/10.1029/2007JB005569.

Contreras-Reyes, E., Grevemeyer, I., Watts, A.B., Flueh, E.R., Peirce, C., Moeller, S., Papenberg, C., 2011. Deep seismic structure of the Tonga subduction zone: implications for mantle hydration, tectonic erosion, and arc magmatism. Journal of Geophysical Research 116, 1–18.

Cook, F.A., Van der Velden, A.J., Hall, K.W., 1997. Upper mantle reflectors beneath the SNORCLE transect — images of the base of the lithosphere? In: Cook, F., Erdmer, P. (Eds.), Slave-Northern Cordillera Lithospheric Evolution (SNORCLE) Transect and Cordilleran Tectonics Workshop Meeting. Lithoprobe Report. University of Calgary, pp. 58–62

Csontos, L., 1995. Cenozoic tectonic evolution of the Intra-Carpathian area: a review. Acta Vulcanologica 7, 1–13.

Currie, C.A., Hyndman, R.D., 2006. The thermal structure of subduction zone back arcs. Journal of Geophysical Research 111, B08404.

Dalziel, I.W.D., Lawver, L.A., Norton, I.O., Gahagan, L.M., 2013. The Scotia arc: genesis, evolution, global significance. Annual Review of Earth and Planetary Sciences 41, 767–793. http://dx.doi.org/10.1146/annurev-earth-050212-124155.

DeMets, C., Gordon, R.G., Argus, D.F., 2010. Geologically current plate motions. Geophysical Journal International 181, 1–80. http://dx.doi.org/10.1111/j.1365-246X.2009.04491.x (http://geoscience.wisc.edu/~chuck/MORVEL/plate_vel_calc.php).

ECORS Pyrenees Team, 1988. The ECORS deep reflection seismic survey across the Pyrenees. Nature 331, 508–510.

Eakin, D.H., McIntosh, K.D., Van Avendonk, H.J.A., et al., 2014. Crustal-scale seismic profiles across the Manila subduction zone: the transition from intraoceanic subduction to incipient collision. Journal of Geophysical Research 119, 1–17.

Eberhart-Philips, D., Christensen, D.H., Brocher, T.M., et al., 2006. Imaging the transition from Aleutian subduction to Yakutat collision in central Alaska, with local earthquakes and active source data. Journal of Geophysical Research 111, B11303.

Eberhart-Phillips, D., Bannister, S., 2002. Three-dimensional crustal structure in the Southern Alps region of New Zealand from inversion of local earthquake and active source data. Journal of Geophysical Research 107 (ESE 15-11-ESE 15-20).
Eberhart-Phillips, D., Reyners, M., 1999. Plate interface properties in the northeast Hikurangi subduction zone, New Zealand, from converted seismic waves. Geophysical Research Letters 26, 2565–2568.
England, P.C., Houseman, G.A., 1989. Extension during continental convergence with application to the Tibetan Plateau. Journal of Geophysical Research 94, 17 561–17 579.
England, P., Molnar, P., 1997. Active deformation of Asia: from kinematics to dynamics. Science 278, 647–650.
Fichtner, A., Kennett, B.L., Igel, H., Bunge, H.-P., 2010. Full waveform tomography for radially anisotropic structure: new insights into present and past states of the Australasian upper mantle. Earth and Planetary Science Letters 290, 270–280.
Fischer, K.M., 2002. Waning buoyancy in the crustal roots of old mountains. Nature 417, 933–936.
Font, Y., Liu, C.-S., Schnurle, P., Lallemand, S., 2001. Constraints on backstop geometry of the southwest Ryukyu subduction based on reflection seismic data. Tectonophysics 333, 135–158.
Forsyth, D., Uyeda, S., 1975. On the relative importance of the driving forces of plate motion. Geophysical Journal of the Royal Astronomical Society 43, 163–200.
Fry, B., Eberhart-Phillips, D., Davey, F., 2014. Mantle accommodation of lithospheric shortening as seen by combined surface wave and teleseismic imaging in the South Island, New Zealand. Geophysical Journal International 199, 499–513.
Gerya, T.V., Burg, J.P., 2007. Intrusion of ultramafic magmatic bodies into the continental crust: numerical simulation. Physics of the Earth and Planetary Interiors 160, 124–142.
Gilbert, H., Beck, S., Zandt, G., 2006. Lithospheric and upper mantle structure of central Chile and Argentina. Geophysical Journal International 165 (1), 383–398. http://dx.doi.org/10.1111/j.1365-246X.2006.02867.x.
Gorbatov, A., Widiyantoro, S., Fukao, Y., Gordeev, E., 2000. Signature of remnant slabs in the North Pacific from P-wave tomography. Geophysical Journal International 142, 27–36.
Götze, H.-J., Krause, S., 2002. The Central Andean gravity high, a relic of an old subduction complex? Journal of South American Earth Sciences 14, 799–811.
Grad, M., Keller, G.R., Thybo, H., Guterch, A., 2002. Lower lithospheric structure beneath the Trans-European Suture Zone from POLONAISE'97 seismic profiles. Tectonophysics 360, 153–168.
Green, A.G., Clowes, R.M., Yorath, C.J., Spencer, C., Kanasewich, E.R., Brandon, M.T., Brown, A.S., 1986. Seismic-reflection imaging of the subducting Juan-de-Fuca plate. Nature 319, 210–213.
Grevemeyer, I., Ranero, C.R., Flueh, E.R., Klaeschen, D., Bialas, J., 2007. Passive and active seismological study of bending-related faulting and mantle serpentinization at the Middle America trench. Earth and Planetary Science Letters 258 (3-4), 528–542. http://dx.doi.org/10.1016/j.epsl.2007.04.013.
Hall, R., Spakman, W., 2002. Subducted slabs beneath the eastern Indonesia–Tonga region: insights from tomography. Earth and Planetary Science Letters 201, 321–336.
Hayes, G.P., Wald, D.J., Johnson, R.L., 2012. Slab 1.0: a three-dimensional model of global subduction zone geometries. Journal of Geophysical Research 117, 1–15.
Hirose, F., Nakajima, J., Hasegawa, A., 2008. Three-dimensional seismic velocity structure and configuration of the Philippine Sea slab in southwestern Japan estimated by double-difference tomography. Journal of Geophysical Research: Solid Earth (1978–2012) 113.
Holbrook, W.S., Lizarralde, D., McGeary, S., Bangs, N., Diebold, J., 1999. Structure and composition of the Aleutian island arc and implications for continental crustal growth. Geology 27, 31–34.
Houseman, G.A., Molnar, P., 1997. Gravitational (Rayleigh–Taylor) instability of a layer with non-linear viscosity and convective thinning of continental lithosphere. Geophysical Journal International 128, 125–150.
Hsui, A.T., Xiao-Ming, T., Toksoz, M.N., 1990. On the dip angle of subducting plates. Tectonophysics 179, 163–175.
Hyndman, R.D., Yorath, C.J., Clowes, R.M., Davis, E.E., 1990. The northern Cascadia subduction zone at Vancouver island — seismic structure and tectonic history. Canadian Journal of Earth Sciences 27, 313–329.
IHFC, 2011. The Global Heat Flow Database. International Heat Flow Commission (http://www.heatflow.und.edu/index2.html).
Jagoutz, O., Behn, M.D., 2013. Foundering of lower island-arc crust as an explanation for the origin of the continental Moho. Nature 504, 131–134.
Jiang, G., Zhao, D., Zhang, G., 2009. Seismic tomography of the Pacific slab edge under Kamchatka. Tectonophysics 465, 190–203.
Jicha, B.R., Scholl, D.W., Singer, B.S., et al., 2006. Revised age of Aleutian Island Arc formation implies high rate of magma production. Geology 34 (8), 661–664.
Johnston, S.T., Thorkelson, D.J., 1997. Cocos-Nazca slab window beneath Central America. Earth and Planetary Science Letters 146, 465–474.
Kárason, H., Van Der Hilst, R.D., 2000. Constraints on mantle convection from seismic tomography. The History and Dynamics of Global Plate Motionspp. 277–288.
Kay, R.W., Kay, S.M., 1993. Delamination and delamination magmatism. Tectonophysics 219, 177–189.
Kim, Y., Clayton, R.W., Jackson, J.M., 2010. Geometry and seismic properties of the subducting Cocos plate in central Mexico. Journal of Geophysical Research 115, B06310.
Kind, R., Yuan, X., Saul, J., Nelson, D., Sobolev, S., Mechie, J., Zhao, W., Kosarev, G., Ni, J., Achauer, U., 2002. Seismic images of crust and upper mantle beneath Tibet: evidence for Eurasian plate subduction. Science 298, 1219–1221.
Knapp, J.H., Knapp, C.C., Raileanu, V., Matenco, L., Mocanu, V., Dinu, C., 2005. Crustal constraints on the origin of mantle seismicity in the Vrancea Zone, Romania: the case for active continental lithospheric delamination. Tectonophysics 410, 311–323.
Kodaira, S., Takahashi, N., Nakanishi, A., Miura, S., Kaneda, Y., 2000. Subducted seamount imaged in the rupture zone of the 1946 Nankaido earthquake. Science 289, 104–106.
Kopp, H., Flueh, E.R., Klaeschen, D., Bialas, J., Reichert, C., 2011. Crustal structure of the central Sunda margin at the onset of oblique subduction. Geophysical Journal International 147 (2), 449–474. http://dx.doi.org/10.1046/j.0956-540x.2001.01547.x.
Kosarev, G., Kind, R., Sobolev, S., Yuan, X., Hanka, W., Oreshin, S., 1999. Seismic evidence for a detached Indian lithospheric mantle beneath Tibet. Science 283, 1306–1309.
Koulakov, I., Sobolev, S.V., 2006. A tomographic image of Indian lithosphere break-off beneath the Pamir–Hindukush region. Geophysical Journal International 164, 425–440.
Kushiro, I., 1974. Melting of hydrous upper mantle and possible generation of andesitic magma — an approach from synthetic systems. Earth and Planetary Science Letters 22, 294–299.
Lagabrielle, Y., Maurizot, P., Lafoy, Y., Cabioch, G., Pelletier, B., Régnier, M., Wabete, I., Calmant, S., 2005. Post-Eocene extensional tectonics in Southern New Caledonia (SW Pacific): insights from onshore fault analysis and offshore seismic data. Tectonophysics 403, 1–28.
Lallemand, S., Font, Y., Bijwaard, H., Kao, H., 2001. New insights on 3-D plates interaction near Taiwan from tomography and tectonic implications. Tectonophysics 335, 229–253.
Larter, R.D., Vanneste, L.E., Morris, P., Smythe, D.K., 2003. Structure and tectonic evolution of the South Sandwich arc. Geological Society, London, Special Publications 219, 255–284.
Laske, G., Masters, G., Ma, Z., Pasyanos, M., 2013. Update on CRUST1.0 — a 1-degree global model of earth's crust. Geophysical Research Abstracts 15 (Abstract EGU2013–2658 http://igppweb.ucsd.edu/~gabi/rem.html).
Levander, A., Bezada, M.J., Niu, F., et al., 2014. Subduction-driven recycling of continental margin lithosphere. Nature 515 (253-U219).
Levin, V., Shapiro, N., Park, J., Ritzwoller, M., 2002. Seismic evidence for catastrophic slab loss beneath Kamchatka. Nature 418, 763–767.
Li, C., van der Hilst, R.D., Engdahl, E.R., Burdick, S., 2008. A new global model for P wave speed variations in Earth's mantle. Geochemistry, Geophysics, Geosystems 9.
Lie, J.E., Pedersen, T., Husebye, E.S., 1990. Observations of seismic reflectors in the lower lithosphere beneath the Skagerrak. Nature (London) 346, 165–168.
Lippitsch, R., Kissling, E., Ansorge, J., 2003. Upper mantle structure beneath the Alpine orogen from high-resolution teleseismic tomography. Journal of Geophysical Research: Solid Earth (1978–2012) 108.
Lorinczi, P., Houseman, G., 2009. Lithospheric gravitational instability beneath the Southeast Carpathians. Tectonophysics 486, 150.
Lizarralde, D., Holbrook, W.S., McGeary, S., Bangs, N.L., Diebold, J.B., 2002. Crustal construction of a volcanic arc, wide-angle seismic results from the western Alaska Peninsula. Journal of Geophysical Research 107. http://dx.doi.org/10.1029/2001JB000230.
Lüschen, E., Müller, C., Kopp, H., Engels, M., Lutz, R., Planert, L., Shulgin, A., Djajadihardja, Y., 2011. Structure, evolution and tectonic activity of the eastern Sunda forearc, Indonesia, from marine seismic investigations. Tectonophysics 508, 6–21.
Madsen, J., Thorkelson, D., Friedman, R.M., Marshall, D., 2006. Cenozoic to Recent plate configurations in the Pacific Basin: ridge subduction and slab window magmatism in western North America. Geosphere 2, 11–34.
Matsubara, M., Obara, K., Kasahara, K., 2008. Three-dimensional P-and S-wave velocity structures beneath the Japan Islands obtained by high-density seismic stations by seismic tomography. Tectonophysics 454, 86–103.
McIntosh, K., Nakamura, Y., Wang, T.-K., Shih, R.-C., Chen, A., Liu, C.-S., 2005. Crustal-scale seismic profiles across Taiwan and the western Philippine Sea. Tectonophysics 401, 23–54.
Mezcua, J., Rueda, J., 1997. Seismological evidence for a delamination process in the lithosphere under the Alboran Sea. Geophysical Journal International 129, F1–F8.
Moghadam, H.S., Stern, R.J., 2011. Geodynamic evolution of Upper Cretaceous Zagros ophiolites: formation of oceanic lithosphere above a nascent subduction zone. Geological Magazine 148, 762–801.
Molnar, P., Houseman, G.A., 2004. The effects of buoyant crust on the gravitational instability of thickened mantle lithosphere at zones of intracontinental convergence. Geophysical Journal International 158, 1134–1150.
MONA LISA Working Group, 1997. Closure of the Tornquist sea: constraints from MONA LISA deep seismic reflection data. Geology 25, 1071–1074.
Morais, I., Vinnik, L., Silveira, G., et al., 2015. Mantle beneath the Gibraltar Arc from receiver functions. Geophysical Journal International 200, 1153–1169.
Mueller, R.D., Sdrolias, M., Gaina, C., et al., 2008. Age, spreading rates, and spreading asymmetry of the world's ocean crust. Geochemistry, Geophysics, Geosystems 9, Q04006.
Nagumo, S., Ouchi, T., Kasahara, J., Koresawa, S., Tomoda, Y., Kobayashi, K., Furumoto, A., Odegard, M., Sutton, G., 1981. Sub-Moho seismic profile in the Mariana Basin—ocean bottom seismograph long-range explosion experiment. Earth and Planetary Science Letters 53, 93–102.
Nakamura, Y., Kodaira, S., Cook, B.J., et al., 2014. Seismic imaging and velocity structure around the JFAST drill site in the Japan Trench: low Vp, high Vp/Vs in the transparent frontal prism. Earth, Planets and Space 66 (Article Number: 121).
Nakanishi, A., Kurashimo, E., Tatsumi, Y., Yamaguchi, H., Miura, S., Kodaira, S., Obana, K., Takahashi, N., Tsuru, T., Kaneda, Y., Iwasaki, T., Hirata, N., 2009. Crustal evolution of the southwestern Kuril Arc, Hokkaido Japan, deduced from seismic velocity and geochemical structure. Tectonophysics 472, 105–123.
Nicholson, T., Bostock, M., Cassidy, J., 2005. New constraints on subduction zone structure in northern Cascadia. Geophysical Journal International 161, 849–859.

Nishizawa, A., Kaneda, K., Katagiri, Y., Kasahara, J., 2007. Variation in crustal structure along the Kyushu–Palau Ridge at 15–21 N on the Philippine Sea plate based on seismic refraction profiles. Earth, Planets and Space 59, e17–e20.
Okaya, D., Henrys, S., Stern, T., 2002. Double-sided onshore–offshore seismic imaging of a plate boundary: "super-gathers" across South Island, New Zealand. Tectonophysics 355, 247–263.
Oncken, O., Sobolev, S.V., Stiller, M., et al., 2003. Seismic imaging of a convergent continental margin and plateau in the central Andes (Andean Continental Research Project 1996 (ANCORP' 96)). Journal of Geophysical Research 108, B2328.
Park, J.-O., Tokuyama, H., Shinohara, M., Suyehiro, K., Taira, A., 1998. Seismic record of tectonic evolution and backarc rifting in the southern Ryukyu island arc system. Tectonophysics 294, 21–42.
Pascal, G., Dubois, J., Barazangi, M., Isacks, B.L., Oliver, J., 1973. Seismic velocity anomalies beneath the New Hebrides island arc: evidence for a detached slab in the upper mantle. Journal of Geophysical Research 78, 6998–7004.
Pavlis, N.K., Holmes, S.A., Kenyon, S.C., Factor, J.K., 2012. The development and evaluation of the Earth Gravitational Model 2008 (EGM2008). Journal of Geophysical Research 117, B04406. http://dx.doi.org/10.1029/2011JB008916.
Platt, J., Vissers, R., 1989. Extensional collapse of thickened continental lithosphere: a working hypothesis for the Alboran Sea and Gibraltar arc. Geology 17, 540–543.
Qorbani, E., Bianchi, I., Bokelmann, G., 2015. Slab detachment under the Eastern Alps seen by seismic anisotropy. Earth and Planetary Science Letters 409, 96–108.
Replumaz, A., Karason, H., van der Hilst, R.D., Besse, J., Tapponnier, P., 2004. 4-D evolution of SE Asia's mantle from geological reconstructions and seismic tomography. Earth and Planetary Science Letters 221 (1-4), 103–115. http://dx.doi.org/10.1016/S0012-821X(04)00070-6.
Reyners, M., Eberhart-Phillips, D., Stuart, G., Nishimura, Y., 2006. Imaging subduction from the trench to 300 km depth beneath the central North Island, New Zealand, with Vp and Vp/Vs. Geophysical Journal International 165, 565–583.
Rogers, R.D., Kárason, H., van der Hilst, R.D., 2002. Epeirogenic uplift above a detached slab in northern Central America. Geology 30, 1031–1034.
Rondenay, S., Abers, G.A., Van Keken, P.E., 2008. Seismic imaging of subduction zone metamorphism. Geology 36, 275–278.
Rudnick, R.L., 1995. Making continental crust. Nature 378, 571–577.
Sarker, G., Abers, G.A., 1998. Deep structures along the boundary of a collisional belt: attenuation tomography of P and S waves in the Greater Caucasus. Geophysical Journal International 133, 326–340.
Schaeffer, A., Lebedev, S., 2013. Global shear speed structure of the upper mantle and transition zone. Geophysical Journal International 194, 417–449.
Schellart, W.P., Rawlinson, N. (Eds.), 2010. Convergent Plate Margin Dynamics: New Perspectives From Structural Geology, Geophysics and Geodynamic Modelling. Tectonophysics 483, pp. 1–190.
Schurr, B., Rietbrock, A., Asch, G., Kind, R., Oncken, O., 2006. Evidence for lithospheric detachment in the central Andes from local earthquake tomography. Tectonophysics 415, 203–223.
Sengör, A.M.C., Natal'in, B.A., 1996. Paleotectonics of Asia: fragments of a synthesis. In: Yin, A., Harrison, T.M. (Eds.), The Tectonic Evolution of Asia. Cambridge University Press, Cambridge, UK, pp. 486–640.
Shomali, Z.H., Roberts, R.G., Pedersen, L.B., Grp, T.O.R.W., 2006. Lithospheric structure of the Tornquist Zone resolved by nonlinear P and S teleseismic tomography along the TOR array. Tectonophysics 416, 133–149.
Shulgin, A., Kopp, H., Mueller, C., et al., 2009. Sunda-Banda arc transition: incipient continent–island arc collision (northwest Australia). Geophysical Research Letters 36, L10304.
Shulgin, A., Kopp, H., Mueller, C., Planert, L., Lueschen, E., Flueh, E., Djajadihardja, Y., 2011. Structural architecture of oceanic plateau subduction offshore Eastern Java and the potential implications for geohazards. Geophysical Journal International 184, 12–28.
Shulgin, A., Kopp, H., Klaeschen, D., et al., 2013. Subduction system variability across the segment boundary of the 2004/2005 Sumatra megathrust earthquakes. Earth and Planetary Science Letters 365, 108–119.
Sizova, E., Gerya, T., Brown, M., Perchuk, L.L., 2010. Subduction styles in the Precambrian: insight from numerical experiments. Lithos 116, 209–229.
Souriau, A., Chevrot, S., Olivera, C., 2008. A new tomographic image of the Pyrenean lithosphere from teleseismic data. Tectonophysics 460, 206–214.
Spakman, W., Hall, R., 2010. Surface deformation and slab–mantle interaction during Banda arc subduction rollback. Nature Geoscience 3, 562–566.
Spakman, W., Wortel, M., Vlaar, N., 1988. The Hellenic subduction zone: a tomographic image and its geodynamic implications. Geophysical Research Letters 15, 60–63.
Spakman, W., van der Lee, S., van der Hilst, R., 1993. Travel-time tomography of the European–Mediterranean mantle down to 1400 km. Physics of the Earth and Planetary Interiors 79, 3–74.
Sperner, B., Lorenz, F., Bonjer, K., et al., 2001. Slab break-off — abrupt cut or gradual detachment? New insights from the Vrancea Region (SE Carpathians, Romania). Terra Nova 13, 172–179.
Starostenko, V., Janik, T., Kolomiyets, K., et al., 2013. Seismic velocity model of the crust and upper mantle along profile PANCAKE across the Carpathians between the Pannonian Basin and the East European Craton. Tectonophysics 608, 1049–1072.
Stauffer, P., 1993. Deep seismic reflection evidence for continental underthrusting beneath southern Tibet. Nature 366, 9.
Stern, T., Smith, E., Davey, F., Muirhead, K., 1987. Crustal and upper mantle structure of the northwestern North Island, New Zealand, from seismic refraction data. Geophysical Journal International 91, 913–936.
Stern, T.A., Henrys, S.A., Okaya, D., et al., 2015. A seismic reflection image for the base of a tectonic plate. Nature 518, 85–89.
Storchak, D.A., Di Giacomo, D., Bondár, I., Engdahl, E.R., Harris, J., Lee, W.H.K., Villaseñor, A., Bormann, P., 2013. Public release of the ISC-GEM global instrumental earthquake catalogue (1900–2009). Seismological Research Letters 84 (5), 810–815.
Stratford, W., Peirce, C., Paulatto, M., et al., 2015. Seismic velocity structure and deformation due to the collision of the Louisville Ridge with the Tonga–Kermadec Trench. Geophysical Journal International 200, 1503–1522.
Suyehiro, K., Takahashi, N., Ariie, Y., Yokoi, Y., Hino, R., Shinohara, M., Kanazawa, T., Hirata, N., Tokuyama, H., Taira, A., 1996. Continental crust, crustal underplating, and low-Q upper mantle beneath an oceanic island arc. Science 272, 390–392.
Taira, A., Saito, S., Aoike, K., Morita, S., Tokuyama, H., Suyehiro, K., Takahashi, N., Shinohara, M., Kiyokawa, S., Naka, J., Klaus, A., 1998. Nature and growth rate of the northern Izu-Bonin (Ogasawara) arc crust and their implications for continental crust formation. Island Arc 7, 395–407.
Takahashi, N., Kodaira, S., Tatsumi, Y., et al., 2008. Structure and growth of the Izu–Bonin–Mariana arc crust: 1. Seismic constraint on crust and mantle structure of the Mariana arc–back-arc system. Journal of Geophysical Research 113 (B1). http://dx.doi.org/10.1029/2007JB005120.
Taylor, S.R., 1967. The origin and growth of continents. Tectonophys. 4, 17–34.
Thybo, H., Artemieva, I.M., 2013. Moho and magmatic underplating in continental lithosphere. Tectonophysics 609, 605–619.
Tatsumi, Y., 2005. The subduction factory: How it operates in the evolving Earth. GSA Today 15, 4–10.
Tilmann, F.J., INDEPTH III Seismic Team, Ni, J., 2003. Seismic imaging of the downwelling Indian lithosphere beneath central Tibet. Science 300, 1424–1427.
Trehu, A.M., Asudeh, I., Brocher, T.M., Luetgert, J.H., Mooney, W.D., Nabelek, J.L., Nakamura, Y., 1994. Crustal architecture of the Cascadia fore-arc. Science 266, 237–243.
Trenkamp, R., Kellogg, J.N., Freymueller, J.T., Mora, H.P., 2002. Wide plate margin deformation, southern Central America and northwestern South America, CASA GPS observations. Journal of South American Earth Sciences 15, 157–171.
Turner, S., Hawkesworth, C., Liu, J., Rogers, N., Kelley, S., van Calsteren, P., 1993. Timing of Tibetan uplift constrained by analysis of volcanic rocks. Nature 364, 50–54.
UNESCO Project 600. Project 600 — metallogenesis of collisional orogenshttp://www.unesco.org/new/en/natural-sciences/environment/earth-sciences/international-geoscience-programme/igcp-projects/earth-resources/project-600-sida/.
Uyeda, S., Kanamori, H., 1979. Back-arc opening and the mode of subduction. Journal of Geophysical Research 84, 1049–1061.
Vacher, P., Souriau, A., 2001. A three-dimensional model of the Pyrenean deep structure based on gravity modelling, seismic images and petrological constraints. Geophysical Journal International 145, 460–470.
Van Avendonk, H.J., Holbrook, W.S., Okaya, D., Austin, J.K., Davey, F., Stern, T., 2004. Continental crust under compression: a seismic refraction study of South Island Geophysical Transect I, South Island, New Zealand. Journal of Geophysical Research: Solid Earth (1978–2012) 109.
Van der Voo, R., Spakman, W., Bijwaard, H., 1999a. Tethyan subducted slabs under India. Earth and Planetary Science Letters 171, 7–20.
Van der Voo, R., Spakman, W., Bijwaard, H., 1999b. Mesozoic subducted slabs under Siberia. Nature 397, 246–249.
Wada, I., Wang, K., 2009. Common depth of slab–mantle decoupling: reconciling diversity and uniformity of subduction zones. Geochemistry, Geophysics, Geosystems 10, Q10009. http://dx.doi.org/10.1029/2009GC002570.
Wagner, D., Koulakov, I., Rabbel, W., Luehr, B.-G., Wittwer, A., Kopp, H., Bohm, M., Asch, G., 2007. Joint inversion of active and passive seismic data in Central Java. Geophysical Journal International 170, 923–932.
Warner, M., Morgan, J., Barton, P., Morgan, P., Price, C., Jones, K., 1996. Seismic reflections from the mantle represent relict subduction zones within the continental lithosphere. Geology (Boulder) 24, 39–42.
Widiyantoro, S., Kennett, B., Van Der Hilst, R., 1999. Seismic tomography with P and S data reveals lateral variations in the rigidity of deep slabs. Earth and Planetary Science Letters 173, 91–100.
Wittlinger, G., Vergne, J., Tapponnier, P., et al., 2004. Teleseismic imaging of subducting lithosphere and Moho offsets beneath western Tibet. Earth and Planetary Science Letters 221, 117–130.
Wortel, M.J.R., Spakman, W., 2000. Subduction and slab detachment in the Mediterranean–Carpathian region. Science 290, 1910–1917.
Wu, Y.-M., Shyu, J.B.H., Chang, C.-H., Zhao, L., Nakamura, M., Hsu, S.-K., 2009. Improved seismic tomography offshore northeastern Taiwan: implications for subduction and collision processes between Taiwan and the southernmost Ryukyu. Geophysical Journal International 178, 1042–1054.
Xiao, W., Windley, B.F., Allen, M.B., et al., 2013. Paleozoic multiple accretionary and collisional tectonics of the Chinese Tian Shan orogenic collage. Gondwana Research 23, 1316–1341.
Yao, H., van der Hilst, R.D., de Hoop, M.V., 2006. Surface-wave array tomography in SE Tibet from ambient seismic noise and two-station analysis — I. Phase velocity maps. Geophysical Journal International 166, 732–744.
Yokokura, T., 1981. On subduction zone angles. Tectonophysics 77, 63–77.
Yuan, X., Sobolev, S., Kind, R., Oncken, O., Bock, G., Asch, G., Schurr, B., Graeber, F., Rudloff, A., Hanka, W., 2000. Subduction and collision processes in the Central Andes constrained by converted seismic phases. Nature 408, 958–961.
Zatman, S., Gordon, R., Mutnuri, K., 2004. Dynamics of diffuse oceanic plate boundaries: insensitivity to rheology. Geophysical Journal International 162, 239–248.
Zelt, C.A., Hojka, A.M., Flueh, E.R., McIntosh, K.D., 1999. 3D simultaneous seismic refraction and reflection tomography of wide-angle data from the Central Chilean Margin. Geophysical Research Letters 26, 2577–2580.
Zhang, H., Zhao, D., Zhao, J., Xu, Q., 2012. Convergence of the Indian and Eurasian plates under eastern Tibet revealed by seismic tomography. Geochemistry, Geophysics, Geosystems 13.

Zhao, W., Mechie, J., Brown, L., Guo, J., Haines, S., Hearn, T., Klemperer, S., Ma, Y., Meissner, R., Nelson, K., 2001. Crustal structure of central Tibet as derived from project INDEPTH wide-angle seismic data. Geophysical Journal International 145, 486–498.
Zhu, H., Bozdag, E., Peter, D., et al., 2012. Structure of the European upper mantle revealed by adjoint tomography. Nature Geoscience 5, 493–498.
Zielhuis, A., Nolet, G., 1994. Deep seismic expression of an ancient plate boundary in Europe. Science 265, 79–81.

Irina Artemieva is a professor in solid Earth geophysics at the University of Copenhagen, Denmark. She is the author of a recent 794 page-long monograph with Cambridge University Press "*The lithosphere: An interdisciplinary approach*" (2011), co-editor of several special volumes, including a 734 page-long Elsevier volume "*Moho: 100 years after Andrija Mohorovičić*" (2013), and (co)author of research papers on diverse aspects of continental dynamics, thermal regime of the continents, and structure of the continental crust and lithospheric mantle. Irina Artemieva is an elected member of the *Academia Europaea*, *the Royal Danish Academy of Sciences and Letters*, a Fellow of the *Geological Society of America* and of *Royal Astronomical Society*, London. She is the Associate Editor of *Nature Science Reports*, *Tectonophysics,* and *Solid Earth* (EGU), and was the Associate Editor of *Journal of Geodynamics*. She is also a member of various national panels in solid Earth geophysics, including national panels in Ireland, Sweden, Portugal, and various research assessments in USA, Canada, Sweden, Russia, and France. Irina Artemieva is the president of Geodynamics Division of the European Geosciences Union.

Hans Thybo is a professor in solid Earth geophysics at the University of Copenhagen, Denmark. He is the author of more than 200 scientific articles, co-editor of 12 special volumes, including a 734 page-long Elsevier volume "*Moho: 100 years after Andrija Mohorovičić*" (2013), and Editor-in-Chief for ca. 180 volumes of *Tectonophysics*. His main research interests include integrated geophysical and geological-tectonic interpretation, tectonophysics, theoretical seismology, and all aspects of applied seismics. Hans Thybo is an elected member of the *Academia Europaea*, the vice-president of the *Royal Danish Academy of Sciences and Letters,* an elected member of the *Danish Academy of Natural Sciences and Royal Norwegian Academy of Sciences and Letters,* a Fellow of the *Geological Society of America* and of *Royal Astronomical Society*, London, and an Overseas Expert for *Chinese Academy of Sciences*. Hans Thybo is the Associate Editor of *Solid Earth* (EGU), *Journal of Applied Geophysics, and Geophysical Surveys*, and has been the Editor-in-Chief of *Tectonophysics* for nearly 15 years. He is a member of various national panels in solid Earth geophysics, including national panels in Denmark, Sweden, Portugal, and various research assessments in many countries. Among other professional posts, Hans Thybo has been the Seismology Division president and General Secretary of the *European Geosciences Union*, a member of Scientific Advisory Board for *International Continental Drilling Programme*, a Council member of *European Plate Observatory System*, and a member of the *ERC Starting Grant Panel*. Hans Thybo is the President of the *European Geosciences Union*.

Alexey Shulgin is a postdoctoral Fellow at Centre for Earth Evolution and Dynamics (CEED), University of Oslo (Norway). He has received his master degree in geophysics from Lomonosov Moscow State University (Russia) and from UC Berkeley (USA), and PhD (2012) from Helmholtz Institute of Marine Research GEOMAR (Germany), where he also worked as a postdoctoral researcher. He has spent more than twelve months in geophysical marine expeditions in the Indian, Atlantic, and Arctic oceans, as well as in the Mediterranean and Black seas. He also took part in nine large onshore seismic experiments in USA and Europe. His research interests include integrated wide-angle refraction/reflection seismology, shallow reflection seismics, regional seismic tomography, and potential fields modeling. The focus of his research is on the structure of the Java subduction zone, evolution of the Barents sea shelf, crustal structure of aseismic oceanic ridges and continental rifts. Alexey Shulgin has been invited as the speaker and co-convener at the *European Geosciences Union* General Assemblies, and is a recipient of personal two-year postdoctoral research grant from the Danish Research Council. He is a reviewer to several international journals and has (co)authored 10 research peer-review papers.